

UNIVERSITY OF CALGARY

An Analysis of Seismic Wavelet Estimation

by

Ayon Kumar Dey

A THESIS

SUBMITTED TO THE FACULTY OF GRADUATE STUDIES

IN PARTIAL FULFILMENT OF THE REQUIREMENTS FOR THE

DEGREE OF MASTER OF SCIENCE

DEPARTMENT OF GEOLOGY AND GEOPHYSICS

CALGARY, ALBERTA

NOVEMBER 1999

©Ayon Kumar Dey 1999



**National Library  
of Canada**

**Acquisitions and  
Bibliographic Services**

**395 Wellington Street  
Ottawa ON K1A 0N4  
Canada**

**Bibliothèque nationale  
du Canada**

**Acquisitions et  
services bibliographiques**

**395, rue Wellington  
Ottawa ON K1A 0N4  
Canada**

*Your file / Votre référence*

*Our file / Notre référence*

**The author has granted a non-exclusive licence allowing the National Library of Canada to reproduce, loan, distribute or sell copies of this thesis in microform, paper or electronic formats.**

**The author retains ownership of the copyright in this thesis. Neither the thesis nor substantial extracts from it may be printed or otherwise reproduced without the author's permission.**

**L'auteur a accordé une licence non exclusive permettant à la Bibliothèque nationale du Canada de reproduire, prêter, distribuer ou vendre des copies de cette thèse sous la forme de microfiche/film, de reproduction sur papier ou sur format électronique.**

**L'auteur conserve la propriété du droit d'auteur qui protège cette thèse. Ni la thèse ni des extraits substantiels de celle-ci ne doivent être imprimés ou autrement reproduits sans son autorisation.**

0-612-49606-6

**Canada**

# Abstract

In seismic exploration, statistical wavelet estimation and deconvolution are standard tools. Both of these processes assume randomness in the seismic reflectivity sequence and also make a minimum phase assumption about the actual wavelet embedded in the trace. The validity of these assumptions is examined by using well-log reflectivity sequences, synthetic seismic traces, and by using a procedure for evaluating the resulting deconvolutions. With real data, wavelet estimations are compared with the in-situ recording of the actual waveform from a vertical seismic profile (VSP). As a result of these investigations, this thesis presents a fairly simple group of tests that can be used to evaluate the validity of the randomness and minimum phase assumptions. From the investigations of seismic data in Alberta, it is concluded that the assumption of reflectivity randomness is less of a problem in deconvolution than other assumptions such as phase and stationarity.

# Acknowledgements

As much as my superego wants to acknowledge just me, myself, and I, this is simply not the case. This body of research is very much a collaborative effort of the many elements that make up my life. First, and foremost, I would like to acknowledge my supervisor Larry Lines. We have a history that predates my graduate studies and I thank you for all your support, guidance, and friendship over the last five years. You were willing to take a chance on me during a time in my life when I was anything but a sure bet. For that I am forever in your debt. Also to be thanked for their support are the Memorial University Seismic Imaging Consortium (MUSIC) and the Consortium for Research in Elastic Wave Exploration Seismology (CREWES) at the University of Calgary. No acknowledgements would be complete without recognizing the social support structure that kept me sane. To my mom, dad, and sister, thanks for understanding. As for the old crew in St. John's and the new crew in Calgary (you all know who you are), I salute you. I would like to complete this by giving a special word of thanks to my biracial pillars of friendship Raj and Kev. Thanks for dealing with all the baggage and reminding me that to live is to be alive inside. You two know that without your support and good old 13, this treatise would have never have happened.

# Dedication

I respectfully dedicate this Master's thesis to my fraternal grandfather. He taught his children to live and that life is not about work or money. Life is about self-respect and a sense of something greater. This was passed on by his children to his grandchildren. Rest assured grandfather that I have kept the faith and until I join the cosmic spirit my mantra shall be **BHARAT MATA KI JOI!**

# Contents

|          |   |           |
|----------|---|-----------|
| <b>1</b> | <b>Introduction and background</b>                      | <b>15</b> |
| 1.1      | Introduction . . . . .                                  | 15        |
| 1.2      | Background . . . . .                                    | 22        |
| 1.2.1    | The convolutional model . . . . .                       | 23        |
| 1.2.2    | Inverse filtering . . . . .                             | 25        |
| 1.2.3    | Least-squares inverse filtering . . . . .               | 25        |
| 1.2.4    | Minimum phase . . . . .                                 | 26        |
| 1.2.5    | Optimum Wiener filters . . . . .                        | 27        |
| <b>2</b> | <b>Analyzing statistical deconvolution</b>              | <b>30</b> |
| 2.1      | Analyzing the randomness assumption . . . . .           | 30        |
| 2.1.1    | Minimum phase methods . . . . .                         | 33        |
| 2.1.2    | Zero phase methods . . . . .                            | 36        |
| 2.2      | Analyzing the phase assumptions . . . . .               | 37        |
| <b>3</b> | <b>The randomness assumption</b>                        | <b>40</b> |
| 3.1      | A proposed test for the randomness assumption . . . . . | 40        |

|          |   |            |
|----------|---|------------|
| 3.2      | Ideal minimum phase synthetic data . . . . .            | 44         |
| 3.3      | Impulse response minimum phase synthetic data . . . . . | 50         |
| 3.4      | Ideal zero phase synthetic data . . . . .               | 54         |
| 3.5      | Impulse response zero phase synthetic data . . . . .    | 58         |
| 3.6      | Integration of VSP data with Vibroseis data . . . . .   | 62         |
| <b>4</b> | <b>The phase assumption</b>                             | <b>67</b>  |
| 4.1      | Proposed tests for the phase assumption . . . . .       | 67         |
| 4.1.1    | model 1 . . . . .                                       | 73         |
| 4.1.2    | model 2 . . . . .                                       | 78         |
| 4.2      | Phase effects on resolving kernels . . . . .            | 82         |
| 4.2.1    | results: model 1 . . . . .                              | 82         |
| 4.2.2    | results: model 2 . . . . .                              | 86         |
| 4.3      | The well-log phase assumption test . . . . .            | 90         |
| 4.3.1    | results: model 1 . . . . .                              | 90         |
| 4.3.2    | results: model 2 . . . . .                              | 94         |
| 4.4      | The phase assumption test . . . . .                     | 97         |
| 4.4.1    | results: model 1 . . . . .                              | 97         |
| 4.4.2    | results: model 2 . . . . .                              | 101        |
| <b>5</b> | <b>Conclusions</b>                                      | <b>104</b> |

# List of Figures

|     |  |    |
|-----|--|----|
| 1.1 | The result of deconvolution when the wavelet is known (from S.E.G. inversion course notes, B. Russell). . . . .  | 21 |
| 1.2 | The result of deconvolution when an incorrect assumption about wavelet phase is made (from S.E.G. inversion course notes, B. Russell). . . . .                 | 21 |
| 3.1 | Test for reflectivity assumption's effect on wavelet deconvolution. . . . .  | 41 |
| 3.2 | Test for reflectivity assumption's effect on trace deconvolution. . . . .  | 42 |
| 3.3 | A primaries only minimum-phase synthetic trace and the model wavelet. . .  | 47 |
| 3.4 | The trace autocorrelation and the model wavelet autocorrelation. . . . .   | 47 |
| 3.5 | The model wavelet, a Wiener-Levinson double inverse (WLDI) estimate of the wavelet, and a Hilbert transform estimate of the wavelet. . . . .                   | 48 |
| 3.6 | Model, Wiener-Levinson, and Hilbert wavelet deconvolutions. . . . .  | 48 |
| 3.7 | The actual well-log derived reflectivity series, the Wiener-Levinson reflectivity series estimate, and the Hilbert transform reflectivity series estimate. . . | 49 |
| 3.8 | Cross-correlation of the actual reflectivity series with the Wiener-Levinson reflectivity series and the Hilbert transform reflectivity series. . . . .        | 49 |

|      |  |    |
|------|--|----|
| 3.9  | A primaries with multiples minimum-phase synthetic trace and the model wavelet. . . . .  | 51 |
| 3.10 | The trace autocorrelation and the model wavelet autocorrelation. . . . .   | 51 |
| 3.11 | The model wavelet, a Wiener-Levinson double inverse (WLDI) estimate of the wavelet, and a Hilbert transform estimate of the wavelet. . . . .                   | 52 |
| 3.12 | Model, Wiener-Levinson, and Hilbert wavelet deconvolutions. . . . .  | 52 |
| 3.13 | The actual well-log derived reflectivity series, the Wiener-Levinson reflectivity series estimate, and the Hilbert transform reflectivity series estimate. . . | 53 |
| 3.14 | Cross-correlation of the actual reflectivity series with the Wiener-Levinson reflectivity series and the Hilbert transform reflectivity series. . . . .        | 53 |
| 3.15 | A primaries only zero-phase synthetic trace and the model Ricker wavelet. .  | 55 |
| 3.16 | The trace autocorrelation and model Ricker wavelet autocorrelation. . . . .  | 55 |
| 3.17 | The model wavelet and a Klauder zero-phase estimate of the wavelet. . . . .  | 56 |
| 3.18 | Ricker and Klauder wavelet deconvolutions. . . . .   | 56 |
| 3.19 | The actual well-log derived reflectivity series, the Ricker band limited reflectivity series estimate, and the Klauder reflectivity series estimate. . . . .   | 57 |
| 3.20 | Cross-correlation of the actual reflectivity series with the Ricker band limited reflectivity series and the Klauder reflectivity series. . . . .              | 57 |
| 3.21 | A primaries with multiples zero-phase synthetic section and the model Ricker wavelet used to create it. . . . .  | 59 |
| 3.22 | The trace autocorrelation and the Ricker wavelet autocorrelation. . . . .  | 59 |
| 3.23 | The model wavelet and a Klauder zero-phase estimate of the wavelet. . . . .  | 60 |
| 3.24 | Ricker and Klauder wavelet deconvolutions. . . . .   | 60 |

|      |   |    |
|------|---|----|
| 3.25 | The actual well-log derived reflectivity series, the Ricker band limited reflectivity series estimate, and the Klauder reflectivity series estimate. . . . .        | 61 |
| 3.26 | Cross-correlation of the actual reflectivity series with the Ricker reflectivity series and the Klauder reflectivity series. . . . .                                | 61 |
| 3.27 | Near offset surface data and the in-situ measured wavelet (down going VSP)  | 64 |
| 3.28 | Near offset trace autocorrelation and in-situ wavelet autocorrelation . . . . .   | 64 |
| 3.29 | Truncated measured wavelet and a Klauder zero-phase wavelet. . . . .  | 65 |
| 3.30 | Near offset trace autocorrelation, truncated wavelet autocorrelation, and Klauder wavelet autocorrelation. . . . .  | 65 |
| 3.31 | Measured wavelet deconvolution, truncated wavelet deconvolution, and Klauder wavelet deconvolution. . . . .   | 66 |
| 3.32 | Near offset traces and their convolution with an in-situ, truncated, and Klauder filter. . . . .  | 66 |
| 4.1  | A validity test of wavelet phase assumption. . . . .  | 69 |
| 4.2  | A well-log validity test of wavelet phase assumption. . . . .   | 70 |
| 4.3  | The minimum delay wavelet, $(-1.1 + z)^2(1.75 + z)^{38}$ , and primaries only reflectivity sequence are convolved to give the synthetic trace to the right. . . . . | 75 |
| 4.4  | A mixed delay wavelet, $(1 - 1.1z)^2(1.75 + z)^{38}$ , and a primaries only reflectivity sequence are convolved to give the synthetic trace to the right. . . . .   | 75 |
| 4.5  | A mixed delay wavelet, $(-1.1 + z)^2(1 + 1.75z)^{38}$ , and a primaries only reflectivity sequence are convolved to give the synthetic trace to the right. . . . .  | 76 |

|      |  |    |
|------|--|----|
| 4.6  | The maximum delay wavelet, $(1 - 1.1z)^2(1 + 1.75z)^{38}$ , and primaries only reflectivity sequence are convolved to give the synthetic trace to the right. . . .                                     | 76 |
| 4.7  | The actual minimum delay wavelet (left) for this model, the Hilbert transform minimum delay wavelet estimate (center) for this model and the deconvolution filter (right) estimated from it. . . . .   | 77 |
| 4.8  | The the actual minimum delay wavelet (left) for this model, the Wiener-Levinson minimum delay wavelet estimate (center) for this model and the deconvolution filter (right) estimated from it. . . . . | 77 |
| 4.9  | The minimum delay wavelet, $(-1.35 + z)^2(1.5 + z)^{38}$ , and primaries only reflectivity sequence are convolved to give the synthetic trace to the right. . . .                                      | 79 |
| 4.10 | A mixed delay wavelet, $(1 - 1.35z)^2(1.5 + z)^{38}$ , and a primaries only reflectivity sequence are convolved to give the synthetic trace to the right. . . . .                                      | 79 |
| 4.11 | A mixed delay wavelet, $(-1.35 + z)^2(1 + 1.5z)^{38}$ , and a primaries only reflectivity sequence are convolved to give the synthetic trace to the right. . . . .                                     | 80 |
| 4.12 | The maximum delay wavelet, $(1 - 1.35z)^2(1 + 1.5z)^{38}$ , and primaries only reflectivity sequence are convolved to give the synthetic trace to the right. . . .                                     | 80 |
| 4.13 | The actual minimum delay wavelet (left) for this model, the Hilbert transform minimum delay wavelet estimate (center) for this model and the deconvolution filter (right) estimated from it. . . . .   | 81 |
| 4.14 | The actual minimum delay wavelet (left) for this model, the Wiener-Levinson minimum delay wavelet estimate (center) for this model and the deconvolution filter (right) estimated from it. . . . .     | 81 |

- 4.15 The model minimum delay wavelet,  $(-1.1 + z)^2(1.75 + z)^{38}$ , its deconvolution filter, and its resolving kernel. The optimal spiking position is at *25ms*. . . . 84
- 4.16 A mixed delay version of the model wavelet,  $(1 - 1.1z)^2(1.75 + z)^{38}$ , its deconvolution filter, and its resolving kernel. The optimal spiking position is at *44ms*. . . . 84
- 4.17 Another mixed delay version of the model wavelet,  $(-1.1 + z)^2(1 + 1.75z)^{38}$ , its deconvolution filter, and its resolving kernel. The optimal spiking position is at *36ms*. . . . 85
- 4.18 The maximum delay version of the model wavelet,  $(1 - 1.1z)^2(1 + 1.75z)^{38}$ , its deconvolution filter and its resolving kernel. The optimal spiking position is at *55ms*. . . . 85
- 4.19 The model minimum delay wavelet,  $(-1.35 + z)^2(1.5 + z)^{38}$ , its deconvolution filter, and its resolving kernel. The optimal spiking position is at *36ms*. . . . 88
- 4.20 A mixed delay version of the model wavelet,  $(1 - 1.35z)^2(1.5 + z)^{38}$ , its deconvolution filter and its resolving kernel. The optimal spiking position is at *44ms*. . . . 88
- 4.21 Another mixed delay version of the model wavelet,  $(-1.35 + z)^2(1 + 1.5z)^{38}$ , its deconvolution filter, and its resolving kernel. The optimal spiking position is at *36ms*. . . . 89
- 4.22 The maximum delay version of the model wavelet,  $(1 - 1.35z)^2(1 + 1.5z)^{38}$ , its deconvolution filter and its resolving kernel. The optimal spiking position is at *44ms*. . . . 89

|      |   |    |
|------|---|----|
| 4.23 | The actual reflectivity sequence (left), spiking deconvolution of the minimum delay synthetic trace based on the Wiener–Levinson wavelet (center), and spiking deconvolution of the minimum delay synthetic trace based on the Hilbert wavelet (right). . . . .           | 92 |
| 4.24 | The actual reflectivity sequence (left), spiking deconvolution of the mixed delay synthetic trace based on the Wiener–Levinson wavelet (center), and spiking deconvolution of the mixed delay synthetic trace based on the Hilbert wavelet (right). . . . .               | 92 |
| 4.25 | The actual reflectivity sequence (left), spiking deconvolution of the second mixed delay synthetic trace based on the Wiener–Levinson wavelet (center), and spiking deconvolution of the second mixed delay synthetic trace based on the Hilbert wavelet (right). . . . . | 93 |
| 4.26 | The actual reflectivity sequence (left), spiking deconvolution of the maximum delay synthetic trace based on the Wiener–Levinson wavelet (center), and spiking deconvolution of the maximum delay synthetic trace based on the Hilbert wavelet (right). . . . .           | 93 |
| 4.27 | The actual reflectivity sequence (left), spiking deconvolution of the minimum delay synthetic trace based on the Wiener–Levinson wavelet (center), and spiking deconvolution of the minimum delay synthetic trace based on the Hilbert wavelet (right). . . . .           | 95 |

|      |   |     |
|------|---|-----|
| 4.28 | The actual reflectivity sequence (left), spiking deconvolution of the mixed delay synthetic trace based on the Wiener–Levinson wavelet (center), and spiking deconvolution of the mixed delay synthetic trace based on the Hilbert wavelet (right). . . . .               | 95  |
| 4.29 | The actual reflectivity sequence (left), spiking deconvolution of the second mixed delay synthetic trace based on the Wiener–Levinson wavelet (center), and spiking deconvolution of the second mixed delay synthetic trace based on the Hilbert wavelet (right). . . . . | 96  |
| 4.30 | The actual reflectivity sequence (left), spiking deconvolution of the maximum delay synthetic trace based on the Wiener–Levinson wavelet (center), and spiking deconvolution of the maximum delay synthetic trace based on the Hilbert wavelet (right). . . . .           | 96  |
| 4.31 | The actual minimum phase wavelet used to create the previously shown synthetic is convolved with the deconvolution filter, estimated from the synthetic trace, to give the resolving kernel to the right. . . . .   | 99  |
| 4.32 | The actual mixed phase wavelet used to create the previously shown synthetic is convolved with the deconvolution filter, estimated from the synthetic trace, to give the resolving kernel to the right. . . . .   | 99  |
| 4.33 | The actual mixed phase wavelet used to create the previously shown synthetic is convolved with the deconvolution filter, estimated from the synthetic trace, to give the resolving kernel to the right. . . . .   | 100 |

|      |   |     |
|------|---|-----|
| 4.34 | The actual maximum phase wavelet used to create the previously shown synthetic is convolved with the deconvolution filter to give the resolving kernel to the right. . . . .                                      | 100 |
| 4.35 | The actual minimum phase wavelet used to create the previously shown synthetic is convolved with the deconvolution filter, estimated from the synthetic trace, to give the resolving kernel to the right. . . . . | 102 |
| 4.36 | The actual mixed phase wavelet used to create the previously shown synthetic is convolved with the deconvolution filter, estimated from the synthetic trace, to give the resolving kernel to the right. . . . .   | 102 |
| 4.37 | The actual mixed phase wavelet used to create the previously shown synthetic is convolved with the deconvolution filter, estimated from the synthetic trace, to give the resolving kernel to the right. . . . .   | 103 |
| 4.38 | The actual maximum phase wavelet used to create the previously shown synthetic is convolved with the deconvolution filter, estimated from the synthetic trace, to give the resolving kernel to the right. . . . . | 103 |

# Chapter 1

## Introduction and background

### 1.1 Introduction

The processing of a digital seismic section is one of the most widely practiced activities in the field of exploration seismology. Signal deconvolution is a processing step that is ideally carried out after exponential gain recovery and before velocity analysis. The underlying purpose of deconvolution is to improve data resolution (i.e. improve the ability to separate two features that are close together, from Sheriff (1974)) by increasing the sharpness of the seismic reflections. In practice, this process attempts to shorten the seismic wavelet, broaden the wavelet's spectrum, remove the change in wavelet shape due to earth filtering, and to stabilize the wavelet from trace to trace.

In both academia and industry, seismic data processors tend to focus on the seismic wavelet when considering the deconvolution problem because if the wavelet is reliably estimated, it can generally be *deconvolved* or shaped to some desired output with a digital

filter. Since the onset of the digital recording, a time honored tradition has arisen in that statistical estimation methods are used to model the seismic wavelet. Although these methods have been in use for several decades, it was only in 1991 that Ziolkowski (February 1991, *Geophysics*) gave a scathing criticism of their theoretical basis. Even though these statistical methods are tried and tested, there has been no comprehensive response to the questions raised by Ziolkowski. The major points of contention arise from the validity of the following statements.

1. The seismic reflectivity sequence is random.
2. The seismic wavelet is minimum phase for impulsive sources and zero phase for vibroseis sources.
3. The seismic wavelet is stationary.

Ziolkowski does not accept the validity of these assumptions. Furthermore, he goes on to propose that seismic wavelets should be modeled on data gathered from direct source measurements.

The problem as it stands now is that the determination of the seismic wavelet via the traditional method of statistical estimation has been challenged and an alternate method has been suggested. This thesis will bring together a comprehensive and detailed analysis of the first two assumptions. The third assumption is addressed in the M.Sc. thesis of Alana Schoepp. All of this will first be considered in a synthetic framework and will then be examined with real data. The importance of this evaluation is that the increased resolution resulting from deconvolution is directly dependent on the wavelet used. Consider Figure

1. This shows that if the wavelet is known, then deconvolution will give consistently good results. Hence, the deconvolution of data is only effective if the estimated wavelet is a reasonable approximation of the true wavelet. To establish the best, and most effective, means of wavelet extraction is key to creating a more interpretable seismic section. This is why the assumptions of statistical wavelet estimation must be tested. The stated problem will be addressed in the following systematic manner.

The first point to be investigated will be the randomness assumption. Statistical wavelet estimation methods assume that the reflectivity is random (i.e. the reflectivity has a probability of occurrence determined by a probability distribution) and this effectively means that the seismic trace autocorrelation is approximately equal to the seismic wavelet autocorrelation. The random reflectivity assumption allows one to estimate the wavelet's autocorrelation, and consequently the amplitude spectrum, from the trace autocorrelation. This thesis develops tests for the randomness assumption. The validity of this assumption can be tested by using sonic and density logs to compute the reflectivity for a series of geological areas. This well log information will allow a measure of the assumption's goodness to be obtained by comparing wavelet estimates obtained by statistical methods, such as the Wiener-Levinson double inverse method and the Hilbert transform method, to the information gained from the well log. This well log information will allow a measure of the assumption's goodness to be obtained by comparing statistical wavelet estimates to the actual wavelet in the case of model data and to information from logs or vertical seismic profiles in the case of real data. The comparison will consider how the trace's autocorrelation relates to the known wavelet's autocorrelation. Then investigations into how this relation differs when statistical

wavelet estimates are used will be done. For synthetic data, a comparison of the model wavelet and wavelet estimates obtained by this assumption will be made. It is expected that the randomness assumption for a reflectivity sequence will be closely tied to the lithology of an area. That is to say, if an exploration area has periodic physical properties, then its reflectivity will not be random. The reflectivity sequence, in this case, violates the randomness assumption because the periodicity of physical properties implies periodic (not random) reflections occurring on a seismogram. The present methods, under the assumption of randomness, would be told to interpret these events as multiples and remove them. This is not the desired effect since processing hopes to image the geology, not obscure it. The end result is a simple test that can be performed on the data to see if there are significant amounts of periodicity which make the randomness assumption invalid. One such way of testing data for randomness is to deconvolve the data with the estimated wavelet and compare the output to the reflectivity derived from well log data or known from a model. The comparison will be done by cross-correlating the reflectivity with the deconvolution output. A 100% perfect deconvolution will have output that cross-correlates with the reflectivity to give a spike. Therefore, it can be said that if this cross-correlation value is within a scale factor of the spike, then the data is random. The exact determination of the scale factor shall result from the investigation of various cases. Practically, this ideal is not often the case since there may be extraneous energy (side lobes, multiples, etc ...) present. Other avenues to be explored with synthetic data include the use of various known wavelets and the use of a reflectivity sequence (a signal that consists of only primary arrivals) instead of an impulse response (a

signal that contains primary and multiple arrivals).

The next issue to be discussed is the problem of estimating the phase spectrum. The randomness assumption allows for the estimation of the wavelet's amplitude spectrum. In order to completely define the wavelet, the phase spectrum is also required. The phase spectrum is often determined by using a minimum phase wavelet (for dynamite sources) or a zero phase wavelet (for vibroseis sources). The critical role of phase estimation in deconvolution can be established by making comparisons between wavelet deconvolutions that make different phase assumptions. Comparisons will allow for an evaluation of this minimum phase assumption. These various deconvolution results will be compared to the reflectivity sequence and evaluated. The evaluation will be done in much the same manner as the test for randomness in that both deconvolution outputs will be cross-correlated with a reflectivity. Whichever gives a result closest to a spike (a perfect cross-correlation is a spike) is the best. It is suspected that the superiority of one over the other will be dependent on the validity of the phase estimates. This comparison and evaluation will occur with a model data set because, with model data, the correct answers are known and therefore the methods can be objectively analyzed. Speaking in a strictly theoretical sense, deconvolution eludes a rigorous mathematical justification because it is the ill-posed problem of one equation and many unknowns. However, these series of investigations hope to evaluate how well these phase assumptions work in practice. To this effect, the deconvolution output will be examined for evidence of distortion, multi-lobed operators, and other effects that are inconsistent with the results of the desired deconvolution. Figure 2 demonstrates what can occur in the output of a deconvolution that makes an incorrect phase assumption about

the seismic wavelet. Establishing the validity of the minimum phase assumption is critical because this is the assumption used for estimating the phase for dynamite and tuned air gun sources.

Ziolkowski's criticism of the wavelet stationarity assumption is the next point to be addressed. Nonstationarity of the wavelet is a reality. It is caused by absorption and dispersion effects in the Earth. These effects are caused by stirring of interstitial pore fluid and constant  $Q$  attenuation. If the data concerned has a nonstationary wavelet for which the assumption of stationarity is invalid, then the amplitude spectrum will show a shift towards the lower frequencies with time. This implies that an empirical evaluation of the assumption will give a limit on the amount of time shift that can occur without violating the stationarity assumption. In theory, if the time varying nature of the wavelet is taken into account, then the estimate of the wavelet should be better. This problem is addressed in Schoepp (1998) and a time variant method is developed.

Outlined above is a problem statement and the groundwork for addressing the problem. This thesis brings the above research to fruition and evaluates the criticisms of statistical deconvolution.

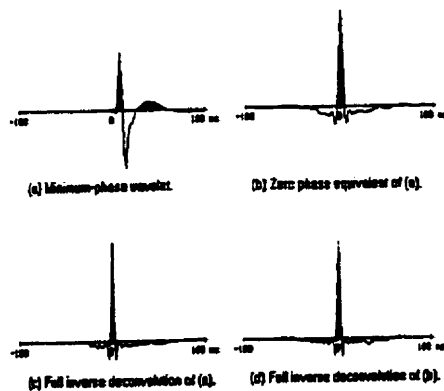


Figure 1.1: The result of deconvolution when the wavelet is known (from S.E.G. inversion course notes, B. Russell).

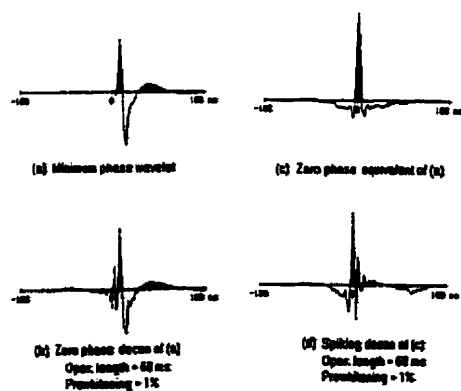


Figure 1.2: The result of deconvolution when an incorrect assumption about wavelet phase is made (from S.E.G. inversion course notes, B. Russell).

## 1.2 Background

Exploration seismologists might think of the earth as being made up of rock layers that have differing lithologies and physical properties. These layers are seismically defined by density and seismic wave propagation velocity, as well as attenuation factors. The product of this velocity and density is the seismic impedance of the layer. Impedance contrasts between adjacent rock layers cause the *reflections* recorded during a seismic survey.

The recorded seismogram can be modeled as the convolution of the earth's impulse response with the seismic wavelet. This impulse response of the earth is what would be recorded if the wavelet were just a delta function or spike. It contains the reflectivity series and all multiples. Ideally, deconvolution compresses the wavelet and removes multiple energy so that only the reflectivity of the primary lithology is left in the recorded seismic trace. The fundamental assumption underlying statistical deconvolution is that of minimum phase because if it is assumed that the seismic wavelet is minimum phase, then its unique phase spectrum can be determined from an input seismic trace. It is because of this (as well as other assumptions) spiking deconvolution is not always desirable.

Deconvolution improves temporal resolution by compressing the basic seismic wavelet. It is normally applied before stack but it is also common to perform deconvolution on post-stack data. After a proper deconvolution, the prominent reflections from interface boundaries are more distinctive because of the compressed waveform and the reduction in the section's ringiness.

### 1.2.1 The convolutional model

A number of assumptions are made to simplify the earth imaging problem described in this work. Six of these are mentioned here and in subsequent areas. The first two of these are as follows.

**Assumption 1** *The earth is comprised of horizontally deposited lithological layers that exhibit constant velocity.*

**Assumption 2** *An impulsive seismic source generates a compressional pressure wave (P-wave) that impinges on lithological layers at normal incidence (i.e., perpendicular to horizontal layer orientation). Physically, this causes no shear waves (S-waves) to be generated as the waveform passes across layer boundaries.*

Assumption 1 is violated in structurally complex areas, such as the foothills of the Canadian Cordillera, and areas that contain gross lateral facies changes. The second of these assumptions implies that zero-offset data must be used but this is a problem since the zero-offset is rarely, if ever, recorded. Both of these assumptions imply that the reflection coefficient  $c$ , for pressure or stress, for the waveform moving from layer 1 to layer 2 can be defined as  $c = \frac{\rho_2 v_2 - \rho_1 v_1}{\rho_2 v_2 + \rho_1 v_1}$ , where  $\rho$  and  $v$  are the densities and velocities of the layers being considered. Assuming a density invariance with depth, within the layers, gives the following approximation  $c \approx \frac{v_2 - v_1}{v_2 + v_1}$ . The reflection coefficient is seen as the ratio of the change in velocity to twice the average velocity.

The P-wave created by an impulsive source is called the signature of the source. All signatures are band-limited wavelets of finite duration. This leads into the next assumption that must be made before an earth model can be put forth.

**Assumption 3** *The source waveform does not change as it travels in the earth's subsurface. That is to say, the seismic source signature is stationary.*

With these three assumptions, the convolutional model of the earth can now be written as:

$$\forall t|t \geq 0, x(t) = w(t) * e(t) + n(t). \quad (1.1)$$

where  $x(t)$  is the recorded seismogram,  $w(t)$  is the seismic source signature,  $e(t)$  is the impulse response of the earth, and  $n(t)$  is random noise. The process of *deconvolution* being discussed seeks to undo this convolution that occurs in the subsurface in order to recover  $e(t)$ . To this end, several more assumptions are made.

**Assumption 4** *The random noise component in a recorded seismogram is zero or can essentially be reduced to zero by processing.*

**Assumption 5** *The seismic source signature, or waveform, is known.*

Again, these assumptions are generally invalid. However, if the latter holds, then the solution to the deconvolution problem is deterministic. Otherwise, the process has only a statistical solution. In the normal run of seismic processing, the signature is rarely known. To ease this assumption, and yet still be able to recover  $e(t)$ , the following assumption is made.

**Assumption 6** *The reflectivity of the earth's subsurface is a random process. This means that the recorded seismogram and the seismic source signature have autocorrelations and amplitude spectra that are identical to within a scale factor.*

### 1.2.2 Inverse filtering

If there is a filter  $a(t)$  such that  $e(t) = a(t) * x(t)$ , then the convolutional model of the earth becomes  $x(t) = w(t) * a(t) * x(t)$ . This model uses the assumption that the noise component is negligible or zero. Simplifying this equation by eliminating  $x(t)$  gives

$$\delta(t) = w(t) * a(t) = \begin{cases} 1 & \text{if } t \text{ equals } 0, \\ 0 & \text{elsewhere.} \end{cases}$$

The function  $\delta(t)$  is the Kronecker delta function and the above simplification implies  $a(t) = \delta(t) * w'(t)$ , where  $w'(t)$  is the inverse wavelet. This means that the operator required to recover the earth's impulse response from a recorded seismogram is the inverse of the seismic source signature. Inverse filtering is a form of deconvolution when this source signature is known. This type of deconvolution is said to be deterministic. Hence, the solution to the deconvolution problem is deterministic (i.e. predictable) when the source wavelet is known. One way to recover the reflectivity in this case is to transform the seismic trace and known wavelet to the frequency domain (via the Fourier transform) and divide. If there are zeros in the transform of the wavelet, then a stability factor  $\epsilon$  is added to the zero and near zero values.

### 1.2.3 Least-squares inverse filtering

The cumulative energy of the error,  $L$ , is defined as the sum of the squares of the differences between the coefficients of the actual and desired outputs. Consider a filter  $(a, b)$  and an input wavelet  $(c, d)$ . The convolution of the two gives the actual output,  $(ac, ad + bc, bd)$ .

In addition, say, the desired output is  $(e, f, g)$ . Then, the cumulative energy of the error between the actual and desired output is  $L = (ac - e)^2 + [(ad + bc) - f]^2 + (bd - g)^2$ . To minimize the error between these coefficients requires that the variation in  $L$  with respect to the filter  $(a, b)$  to vanish. The computation of  $L$  allows for a quantification of goodness. If the desired output has an energy distribution that closely resembles that of the convolved input series, then the error is reduced.

### 1.2.4 Minimum phase

Wavelets are transient waveforms with a finite duration. They can be minimum, maximum, or mixed phase. A minimum phase wavelet has most of its energy at the onset of the time series, while a maximum phase wavelet has most of its energy at the end of the time series. Mixed phase wavelets have their energy distributed throughout the time series. In addition, a wavelet is realizable if it is finite in length (i.e. a finite time series) and is causal if it is zero for all negative times. Hence, a minimum phase wavelet is one that is minimum phase, realizable, and causal. These kinds of wavelets have the least energy delay.

Mathematically, a stable inverse means that the filter coefficients make a convergent series. That is, they decrease with increasing time and vanish at infinity. This means that a stable inverse filter has finite energy. Minimum phase wavelets have stable inverses but maximum and mixed phase wavelets do not. This leads to the following, and final, assumption.

**Assumption 7** *The seismic source wavelet is minimum phase and has a minimum phase inverse.*

Some examples of proven minimum phase phenomena in exploration geophysics are the transmission response of layered media (Robinson and Treitel, 1980) and the attenuation law of Futterman (Futterman, 1962).

### 1.2.5 Optimum Wiener filters

The general form of the matrix equation for an optimum Wiener filter of length  $n$  is  $\mathbf{R}\vec{a} = \vec{g}$ , and the process  $\mathbf{R}^{-1}\mathbf{R}\vec{a} = \mathbf{R}^{-1}\vec{g}$  solves for  $\vec{a}$ . In expanded form (from Robinson and Treitel, 1980):

$$\underbrace{\begin{bmatrix} r_0 & r_1 & \dots & r_{n-1} \\ r_1 & r_0 & \dots & r_{n-2} \\ \vdots & \vdots & \ddots & \vdots \\ r_{n-1} & r_{n-2} & \dots & r_0 \end{bmatrix}}_{\mathbf{R}} \underbrace{\begin{bmatrix} a_0 \\ a_1 \\ \vdots \\ a_{n-1} \end{bmatrix}}_{\vec{a}} = \underbrace{\begin{bmatrix} g_0 \\ g_1 \\ \vdots \\ g_{n-1} \end{bmatrix}}_{\vec{g}} \quad (1.2)$$

where  $\mathbf{R}$  is the autocorrelation matrix of the wavelet which is a symmetric Toeplitz matrix,  $\vec{a}$  is the desired deconvolution filter vector (the vector components are the desired deconvolution filter coefficients), and  $\vec{g}$  is the crosscorrelation vector of the input and desired output. When solving for  $\vec{a}$ , the Toeplitz nature of  $\mathbf{R}$  is exploited by the Wiener-Levinson algorithm to compute the inverse in an efficient manner. The Wiener filter  $\vec{a}$  is optimal in the sense that it least-squares minimizes the energy of the error between actual and desired outputs.

Typically, the desired output is one of the following:

- a spike at arbitrary lag,
- a time advanced form of the input series,
- a zero-phase wavelet,
- or any desired arbitrary shape.

### **spiking deconvolution**

When the process of determining an optimum Wiener filter requires that the desired output be a zero-lag spike, it is called minimum-phase spiking deconvolution. In spiking (or statistical) deconvolution the autocorrelation matrix is computed from the recorded seismogram, while in the case of least-squares inverse filtering (or deterministic deconvolution) this matrix is computed directly from the known source wavelet. If the input wavelet is not minimum phase, then the spiking deconvolution cannot shape the output to a perfect zero-lag spike. This is the pitfall of the minimum phase assumption.

### **prewhitening**

To insure numerical stability (i.e. prevent division by 0) when computing the inverse filter, an artificial level of white noise called prewhitening is introduced to the data before deconvolution. This is achieved by adding a constant to the zero-lag of the autocorrelation function or to the diagonal of  $\mathbf{R}$ .

## shaping filters

For any given wavelet, a series of delayed spikes can be produced as desired output. The least-squares error can then be plotted as a function of delay. The delay, or lag, with the least error is defined to be the desired spike output. Using this spike as the desired output will result, in general, in the Wiener filter producing the most compact result. Wavelet shaping with a spike as the desired output is a special case of shaping deconvolution. Generally speaking, however, shaping deconvolution includes deconvolutions whose desired output is something other than a spike (a narrow Gaussian, for example). In the industry jargon, wavelet shaping filters that result in zero-phase wavelets are called dephasing operators and the process of converting a wavelet to zero-phase is called dephasing (i.e. the desired wavelet is the zero-phase wavelet that could be found from the amplitude spectrum of the input wavelet).

If the input wavelet is the recorded source signature, then wavelet shaping is called signature processing. Wavelet shaping requires a knowledge of the input wavelet. The term wavelet processing generally refers to estimating the embedded wavelet in the seismic data, designing a filter to shape the wavelet to the desired form, and applying the filter to the seismogram.

Minimum phase wavelets have optimal delay at zero, while maximum phase wavelets have optimal delay at wavelet length. To delay the desired spike output, apply a constant time shift to a delayed spike result. Alternatively, shift the shaping filter as much as the delay in the spike and then apply it to the input data. This operator is two-sided (i.e. noncausal) since it has coefficients for positive and negative time values.

# Chapter 2

## Analyzing statistical deconvolution

### 2.1 Analyzing the randomness assumption

The conventional assumptions of wavelet deconvolution have been criticized by some as being generally invalid. One focus of this research is to evaluate the common assumption of reflectivity randomness by use of model synthetics and real data. Since it is expected that this assumption is dependent on geology, data has been examined from various hydrocarbon reservoirs.

Statistical wavelet estimation methods usually assume that the reflectivity is a random uncorrelated signal (that is, the reflectivity has an autocorrelation which approximates a delta function) and this effectively means that the seismic trace autocorrelation,  $T(z)T^*(z)$ , is approximately equal to the seismic wavelet autocorrelation,  $W(z)W^*(z)$ . The deconvolution of data is only effective if the input wavelet is a reasonable approximation to the true wavelet. To establish the best, and most effective, means of wavelet extraction is the key to creating a more interpretable, high-resolution, seismic section. This is precisely why we

must investigate the assumptions upon which our commonly used statistical methods are based. The random reflectivity assumption allows one to estimate the wavelet's autocorrelation, and consequently the amplitude spectrum, from the trace autocorrelation. Hence, given an input seismic trace, it is possible to estimate the wavelet needed for deconvolution.

Four synthetic seismic sections are generated for use in this investigation. Two are created with a minimum phase wavelet and the remaining two are created with a zero phase wavelet. First to be investigated is the validity of the randomness assumption with a primaries only section derived from a well in central Alberta and then with a section that also incorporates multiples, also derived from the same well. The use of synthetic data is done because the wavelet used to generate the section is known and, therefore, meaningful comparisons are made with the statistical estimates.

In judging the accuracy of the randomness assumption, on (model) synthetic data, a systematic approach is developed. Compare the trace autocorrelations with the wavelet autocorrelations and examine the degree of similarity. For a purely random reflectivity, these should be identical to within a scale factor. Subsequently, compare the estimated wavelet with the actual wavelet. However, it is really the deconvolution based on the wavelet estimate that should be evaluated. One way to do this is to compute the convolution of the actual wavelet with the deconvolution filter for the estimated wavelet. One hopes that, this will produce as close a representation of a spike as for the filter computed from the actual wavelet. This estimation of a spike is what is referred to as a *resolving kernel*. That is to say, a resolving kernel is the convolution of a wavelet with a deconvolution filter to get an estimate of the ideal spike. This gives a measure of resolvability in that the convolution of a wavelet with a deconvolution filter should – in the ideal case of estimates that approximate the actual

wavelet well – give a spike as the response. In addition to this, estimates of the reflectivity sequence are generated by convolving the synthetic seismic section with various deconvolution filters. This is simply the deconvolution of the input trace in that the process will remove the wavelet from the input data and the result will be an estimate of the reflectivity sequence. To evaluate how this estimate compares to the well-log derived reflectivity sequence, cross-correlate the two sequences. An ideal cross-correlation of these reflectivities will give a spike as the result. Hence, this can provide a measure of goodness in that comparisons between the similarity of the cross-correlations to a spike can be made.

For the case of real data, the evaluation is somewhat more difficult since the wavelet or the reflectivity sequence is not known. However, there is access to in-situ measurements of the seismic wavelet if there are vertical seismic profile (VSP) data, and in some cases there is also sonic well data to evaluate the deconvolutions. In this particular case, there are vibroseis surface recordings and a VSP recorded from a vibrator source. This allows the actual wavelet to be directly measured as the down-going VSP waveform. It is truncated to the same number of samples as a zero phase wavelet estimate so as to have a measured wavelet with a more reasonable length. Since there is no well-log derived reflectivity sequence to act as a control for the results, the investigation proceeds in a slightly different manner than that used for synthetic data. Instead of comparing estimated sequences to the actual sequence, the results are evaluated with respect to how well responses are brought out and if the ringy nature of the surface data can be suppressed.

### 2.1.1 Minimum phase methods

The estimation of minimum phase wavelets from dynamite data generally use the assumption of a random reflectivity sequence. This assumption is used so that the wavelet's autocorrelation can be derived from the seismic traces's autocorrelation. Given a wavelet's autocorrelation or its corresponding amplitude spectrum, there is then the problem of deriving its phase spectrum. For the case of a minimum phase wavelet, its phase spectrum is uniquely defined by the amplitude spectrum and can be found using either the Wiener-Levinson double inverse method (a time domain method) or the Wold-Kolmogorov factorization method (a frequency domain method). Both of these methods use the assumption of reflectivity randomness to estimate minimum phase wavelets. There is an overview of these methods in the subsections below and detailed descriptions can be found in White and O'Brien (1974), Claerbout (1976), and Lines and Ulrych (1977).

#### The Wiener-Levinson double inverse method

The Wiener filter shapes a time sequence into an approximation of the desired output in a least-squares sense. There is an assumption of wavelet stationarity in this method. It uses this assumption to minimize the square of the difference between the actual output and the desired output by choice of a Wiener filter to get a system of *normal* equations. This system is as follows:

$$\underbrace{\begin{bmatrix} r(0) & r(1) & \dots & r(n) \\ r(1) & r(0) & \dots & r(n-1) \\ \vdots & \vdots & \ddots & \vdots \\ r(n) & r(n-1) & \dots & r(0) \end{bmatrix}}_{\mathbf{R}} \underbrace{\begin{bmatrix} f(0) \\ f(1) \\ \vdots \\ f(n) \end{bmatrix}}_{\vec{f}} = \underbrace{\begin{bmatrix} g(0) \\ g(1) \\ \vdots \\ g(n) \end{bmatrix}}_{\vec{g}}, \text{ where } \forall t \quad (2.1)$$

$$r(n) = \frac{1}{N} \sum_{\tau} x(n+\tau)x(\tau) = \text{input autocorrelation,}$$

$$g(n) = \frac{1}{N} \sum_{\tau} x(\tau)z(n+\tau) = \text{input and desired output cross-correlation,}$$

$$f(n) = \text{the deconvolution filter coefficients, and}$$

$$N = \text{length of the input sequence.}$$

The inverse Wiener filter is designed so that the wavelet estimate is shaped to a spike. This allows for an estimate of the impulse response of a layered earth to be computed by convolving the inverse Wiener filter with the input trace. If the impulse response being estimated is a white noise sequence (that is, random), then the trace autocorrelation can be replaced by the wavelet autocorrelation. It should be noted that this method truncates the trace autocorrelation to obtain this approximation but it can also be accomplished by windowing the trace autocorrelation (e.g. using a Hanning window). In addition, if a zero-delay is the desired output, then only the first component of the cross-correlation vector in the normal equations will be non-zero. A zero-delay spike for desired output is optimal if and only if

the the wavelet being considered is minimum delay. Using these assumptions of a random impulse response and a zero-delay spike as desired output enables a Wiener deconvolution filter to be designed without explicitly evaluating the source wavelet. Estimating the wavelet itself is done by applying the process again to invert the original minimum delay filter and now the output is the minimum phase wavelet estimate.

### The Wold-Kolmogorov factorization method

This is a method where by a minimum phase spectrum is determined from a given amplitude spectrum. If given an amplitude spectrum for a wavelet of length  $n + 1$ , then there are  $2^n$  wavelets with different phase spectra that will have this given amplitude spectrum. However, only one of these  $2^n$  wavelets will have a minimum phase spectrum. By comparing the natural logarithm of the amplitude spectrum,  $\log_e(|W(\omega)|)$ , to the natural logarithm of the wavelet's Fourier transform,  $\log_e(W(\omega))$ , the minimum phase spectrum can be deduced from the amplitude spectrum. As shown by Robinson (1967b), the relationship between phase and amplitude is as follows

$$\text{phase spectrum} = \Theta(\omega)$$

$$= -\frac{2}{\pi} \sum_{t=1}^{t=\infty} \sin(\omega t) \overbrace{\int_0^{\pi} \cos(\omega t) \underbrace{\log_e(|W(\omega)|)}_{\text{log amplitude spectrum}} d\omega}^{\text{inverse Fourier transform of } \log_e(|W(\omega)|)}$$

$$= \text{Hilbert transform of the natural logarithm of the amplitude spectrum.}$$

(2.2)

The inverse Fourier transform,  $\nu(t)$ , of  $\log_e(W(\omega))$  can be written as  $\nu(t) = \nu_e(t) + \nu_o(t)$ .

These components are the even and odd parts of  $\nu(t)$  and the even component,  $\nu_e(t)$ , is the inverse Fourier transform of the log amplitude spectrum,  $\log_e(|W(\omega)|)$ . Requiring that  $\omega(t)$  be minimum phase means that  $\nu(t)$  is causal and this causality means that  $\nu_o(t) = \nu_e(t)\text{sgn}(t)$ . The Fourier transform of  $\nu_o(t)$  is the sine transform  $-\frac{2}{\pi} \sum_{t=1}^{t=\infty} \sin(\omega t)\nu_e(t)$ . Computing this gives  $Im[\log_e(W(\omega))]$  and this is the phase spectrum  $\Theta(\omega)$ . The entire process, just described, is essentially equal to that which is shown in Equation 2.2. This equation is used instead of said process because of the computational speed advantage gained when using the *fast Fourier transform* (FFT).

The phase spectrum,  $\Theta(\omega)$ , can also be computed in the frequency domain by the convolution of  $\log_e(|W(\omega)|)$  and the Fourier transform of  $\text{sgn}(t)$ . This convolution is essentially a Hilbert transform and is the reason why the Wold–Kolmogorov factorization method is commonly referred to as the Hilbert transform method. This method is equivalent to the Wiener–Levinson double inverse method if the Wiener filter has an infinite number of filter points and if the wavelet is considered to be a transient time sequence of finite energy.

### 2.1.2 Zero phase methods

The previous section revolves around minimum phase wavelets. Another common type of wavelet is the zero phase wavelet. When compared to minimum phase wavelets, these zero phase wavelets are symmetrical and are very broad banded in the frequency domain. That being the case, investigations are made into the changes that may occur when a zero phase wavelet is used in the reflectivity analysis. The zero phase wavelets in this study are Ricker and Klauder wavelets that have  $30Hz$  as the dominant frequency. Besides the fact that now

there is a zero phase wavelet, nothing else changes and the analysis proceeds in the same manner as for minimum phase wavelets.

### Klauder wavelets

Vibroseis is based on a concept from chirp radar (Klauder et al., 1964) which was adapted for seismic exploration by Conoco researchers. The source signature,  $s(t)$ , sent into the ground by a vibrator is a lengthy sweep of frequencies. As described by Ristow and Jurzyk (1975), the recorded trace,  $y(t)$ , can be considered as the convolution of  $s(t)$  with the reflectivity,  $r(t)$ , and some earth filter,  $e(t)$ . That is to say,  $y(t) = s(t) * e(t) * r(t)$ . The correlation of this recorded trace with the input trace produces

$$\begin{aligned} x(t) &= s(-t) * y(t) \\ &= s(-t) * s(t) * e(t) * r(t) \\ &= w(t) * e(t) * r(t). \end{aligned} \tag{2.3}$$

Here the autocorrelation of the input sweep  $s(-t) * s(t)$  produces a zero-phase wavelet  $w(t)$ , which is also known as the Klauder wavelet.

## 2.2 Analyzing the phase assumptions

The next, and more problematic, issue of concern is that of phase. As stated in the background section, a fundamental assumption that is made about the seismic source signature (or seismic wavelet) is that it is minimum phase for impulsive sources. While this assumption is essential to the process of statistical signature deconvolution, it is generally accepted

as being invalid. That being the case, it is essential to determine how poor this minimum phase assumption for the seismic wavelet is. In practical terms, it would be worthwhile to know how this assumption affects the deconvolution. To that end, a three pronged approach is taken.

Firstly, the effect of assuming that the wavelet is minimum phase will be investigated with respect to resolving kernels. That is, wavelets of various phase will be given as input to an optimum spiking deconvolution program. This program will determine the optimum spiking position based on the input wavelet and then generate a resolving kernel that is the convolution of the input wavelet and the deconvolution filter predicted from it. Two model wavelet scenarios shall be considered. For both of these models, four wavelets (model wavelet and three permutations) shall be investigated: a model minimum phase wavelet, a mixed phase wavelet (permutation), another mixed phase wavelet (permutation), and a maximum phase wavelet (permutation).

After analyzing the resolving kernels, the investigation will focus on how the minimum phase assumption affects trace deconvolution. Again, the two scenarios that will serve as models to investigate are the wavelets discussed above. For each of these, synthetic seismograms will be generated by convolving the wavelet and permutations discussed above with a primaries only reflectivity sequence. These synthetics will then be used to estimate Hilbert transform and Wiener-Levinson minimum phase wavelets. After this, the wavelets estimated from the synthetic trace will be used to generate deconvolution filters. Convolving these filters with the synthetic trace will give two estimates of the reflectivity sequence used to make the trace. By comparing the three (the actual reflectivity sequence and the two estimates), the effect of the minimum phase assumption will be evaluated. The use of noise-free se-

quences is to show how phase effects trace deconvolution in its simplest case. As complexity in the trace increases (i.e. multiples, noise, etc . . .), the effect of phase compounds.

Finally, there will be an investigation of a proposed test for phase. Here, various synthetic sections are used to statistically compute deconvolution filters. Then the actual wavelet that is used to make the section in question will be convolved with the estimated filter. Comparisons of these results to the ideal result of a spike will allow for further evaluation of the minimum phase assumption made about seismic wavelets. Model 1 uses the minimum phase wavelet  $(-1.1 + z)^2(1.75 + z)^{38}$ , its selected permutations, and a primaries only reflectivity sequence. Model 2 will show results involving the minimum phase wavelet  $(-1.35 + z)^2(1.5 + z)^{38}$ , its selected permutations, and the same reflectivity sequence from model 1.

# Chapter 3

## The randomness assumption

### 3.1 A proposed test for the randomness assumption

An extensive analysis of the assumption that the reflectivity sequence is random has led to the development of two tests for randomness. These two tests to check the validity of the randomness assumption are fairly simple and easy to apply. The first of these tests uses a resolving kernel to evaluate the randomness assumption while the second test uses a well-log derived reflectivity sequence to evaluate the goodness of the assumption. To follow are flow charts that outline how these tests work and then there are pseudocodes for the tests themselves.

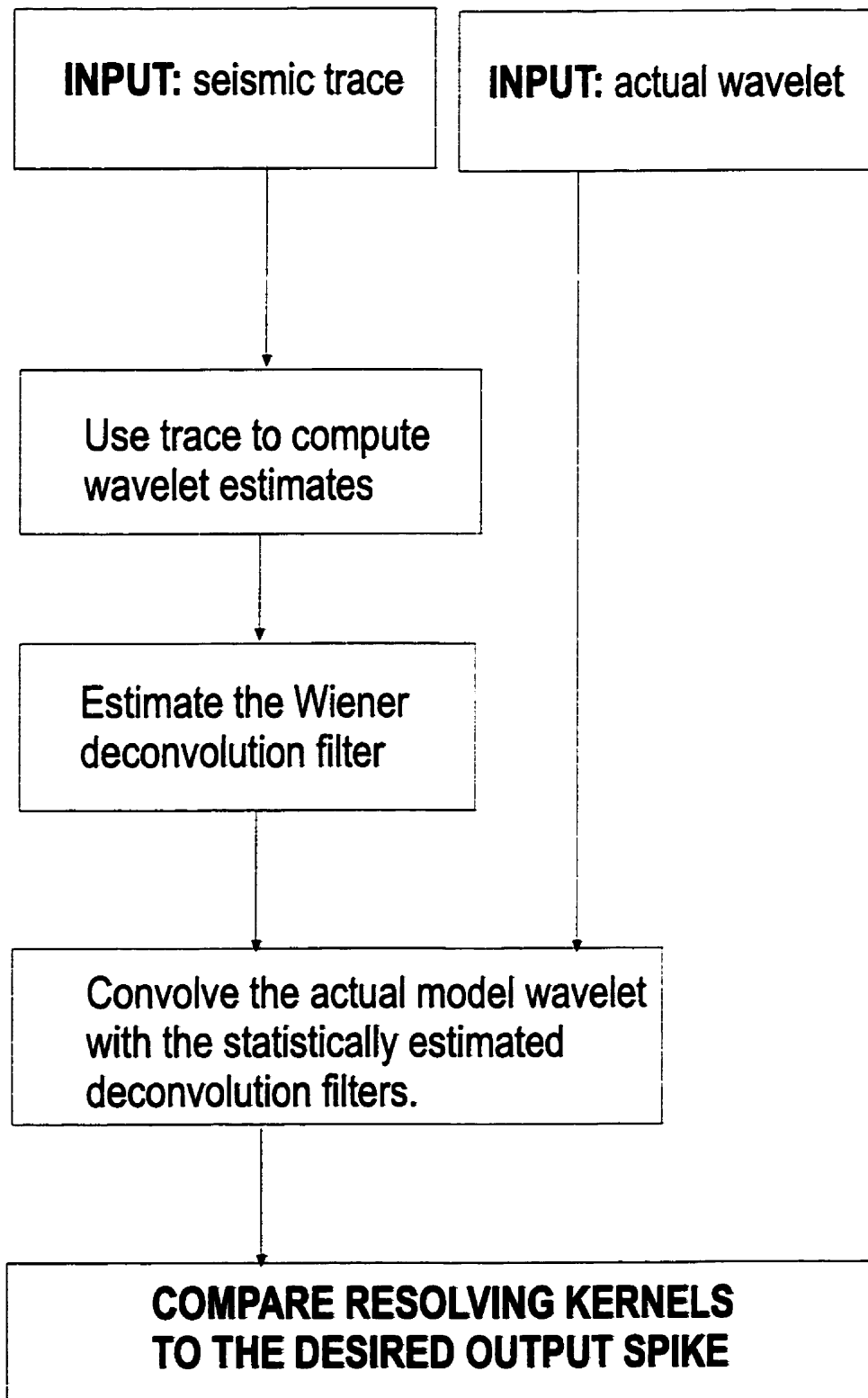


Figure 3.1: Test for reflectivity assumption's effect on wavelet deconvolution.

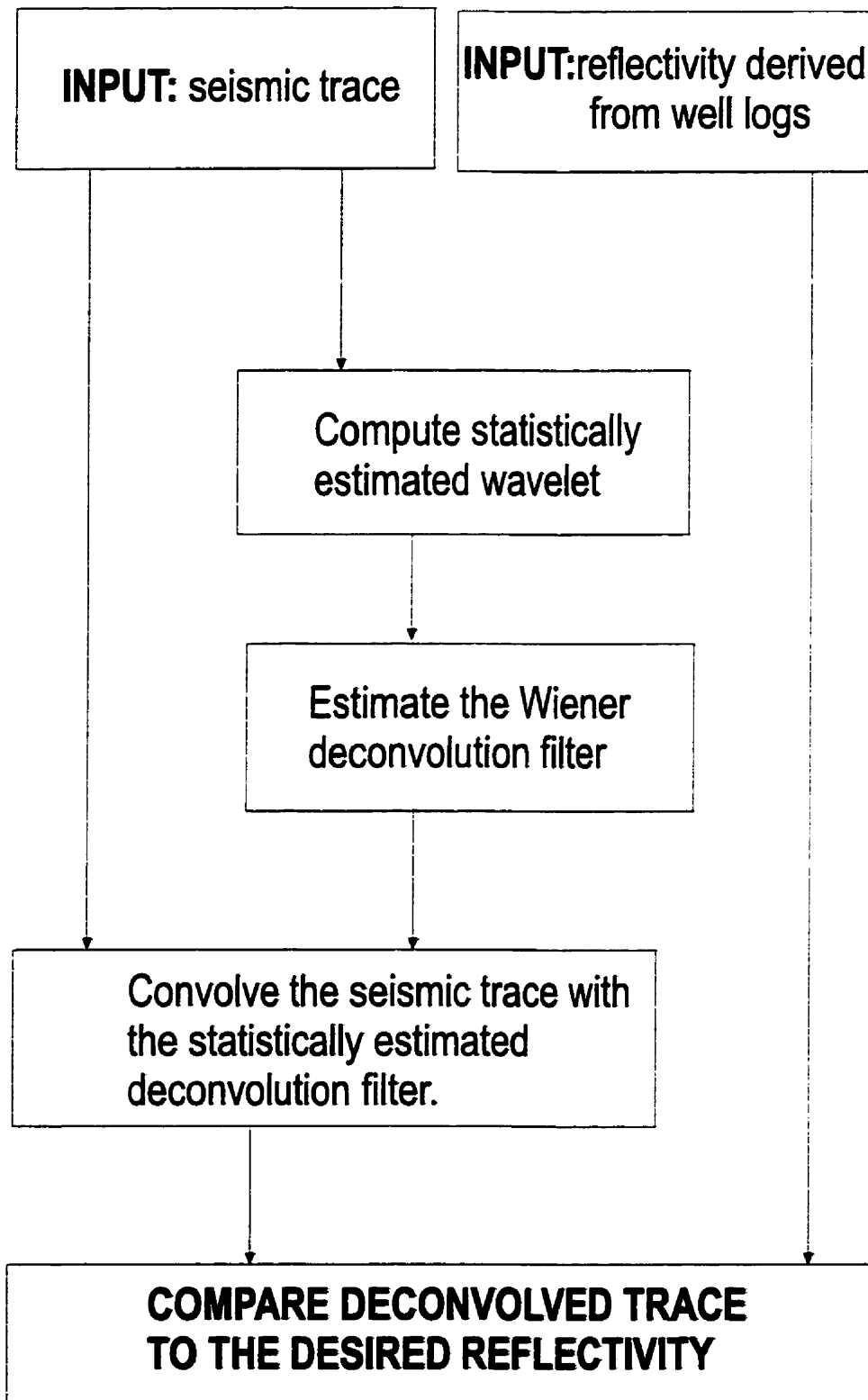


Figure 3.2: Test for reflectivity assumption's effect on trace deconvolution.

**BEGIN:** A validity test for the random reflectivity assumption.

**for each seismic section do**

*compute desired statistically estimated wavelet  $w(n)$ , or  $\vec{w}$ ;*

*compute deconvolution filter  $f(n)$ , or  $\vec{f}$ , based on  $w(n)$  ;*

*compute the resolving kernel;*

*compare to the desired output delta function **end do***

**where**

**proc**  $\vec{w} = (\mathbf{R}^{-1}\vec{g})^{-1}$ ,  $\mathbf{R}$  is the autocorrelation matrix of the trace  $s(n)$ ;

**proc**  $\vec{f} = \mathbf{W}^{-1}\vec{g}$ ,  $\mathbf{W}$  is the autocorrelation matrix of the wavelet;

**proc** resolving kernel  $\equiv \forall n|n \geq 0, w(n) * f(n) = \sum_{\tau=0}^{\tau=N} w(\tau)f(n - \tau)$ .

**END**

**BEGIN:** A well-log validity test for the random reflectivity assumption.

**for each seismic section do**

*compute desired statistically estimated wavelet  $w(n)$ , or  $\vec{w}$ ;*

*compute deconvolution filter  $f(n)$ , or  $\vec{f}$ , based on  $w(n)$ ;*

*compute the trace deconvolution;*

*compare to the well-log derived reflectivity sequence **end do***

**where**

**proc**  $\vec{w} = (\mathbf{R}^{-1}\vec{g})^{-1}$ ,  $\mathbf{R}$  is the autocorrelation matrix of the trace  $s(n)$ ;

**proc**  $\vec{f} = \mathbf{W}^{-1}\vec{g}$ ,  $\mathbf{W}$  is the autocorrelation matrix of the wavelet;

**proc** trace deconvolution  $\equiv \forall n|n \geq 0, s(n) * f(n) = \sum_{\tau=0}^{\tau=N} s(\tau)f(n - \tau)$ .

**END**

The remaining sections of this chapter present a comprehensive set of results regarding the investigations on the randomness assumption. Figures 3.3 through 3.14 illustrate the analysis on minimum phase synthetic sections. Following these are the analyses for the zero phase sections and then the work on real data is displayed.

## 3.2 Ideal minimum phase synthetic data

Shown in Figure 3.3 is a synthetic seismogram that contains only the primary reflections. That is to say, no multiples have been computed. Along side this seismic section is the minimum phase model wavelet used to create it. It is this wavelet that is convolved with a well-log derived reflectivity sequence to generate the synthetic to be analyzed. Note several important reflections between 50 and 100, 100 and 150, and again between 150 and 200. The Wiener-Levinson and Hilbert transform methods base their minimum phase statistical wavelet estimates on an input seismic section. These statistical estimation methods use the trace autocorrelation to reproduce the wavelet autocorrelation under the assumption that the trace autocorrelation is approximately equal to the wavelet autocorrelation. This requires that the reflectivity sequence be random. There is significant similarity between the two plots of trace and wavelet autocorrelations shown in Figure 3.2. The close similarity lends support to the claim of randomness. Now consider the image in Figure 3.5. Here is a comparison of the actual model wavelet and two common minimum phase wavelets. The Hilbert estimate is created from a frequency domain method and the Wiener-Levinson estimate is generated from a time domain method.

Figure 3.6 illustrates the concept of a *resolving kernel*. That is to say, a resolving kernel is the convolution of a model wavelet with a deconvolution filter to get an estimate of the ideal spike. This gives a measure of resolvability in that the convolution of a wavelet with a deconvolution filter should (in the ideal case of estimates that approximate the actual wavelet) give a spike as the response. The deconvolution filter from the model wavelet gives a clean spike. This is to be expected. What is interesting is that the convolutions of the model wavelet with the statistically estimated filters give very good representations of a spike. The result with the Hilbert transform filter has a little noise in the tail and the result from the Wiener–Levinson filter has minute amounts of noise in the tail.

In Figure 3.7, the ability of the statistical methods to reproduce the actual well–log derived reflectivity sequence is evaluated. Using the filters based on statistical estimation, estimates of the reflectivity are generated by convolving the synthetic seismic section with the various filters. This is simply the deconvolution of the input trace in that the process will remove the wavelet from the input data and the result should be the reflectivity. Notice that these deconvolutions are good reproductions of the actual sequence in question. Some things to note are that the estimated reflectivities are a bit smeared and that the estimates have a slight delay. Some significant events that correlate from the actual sequence to the estimated sequences can be noticed just before 50, between 50 and 100, and at about 150. As mentioned before, these events are a bit delayed on the estimates and appear out of phase.

At this stage, the goodness of these reflectivity estimates are examined. Ideally, cross–correlation of the estimated reflectivities with the true reflectivity will give a spike as the result. Hence, the similarity of the cross–correlation to a spike provides a measure of goodness

for the deconvolution. Figure 3.8 shows such a result. Both of the cross-correlations show a spike that is many magnitudes greater than the minor amounts of noise that occur later in the trace. These are accurate estimations of the reflectivity. Notice, again, that there appears to be a slight delay in the cross-correlation with the Hilbert transform estimate.

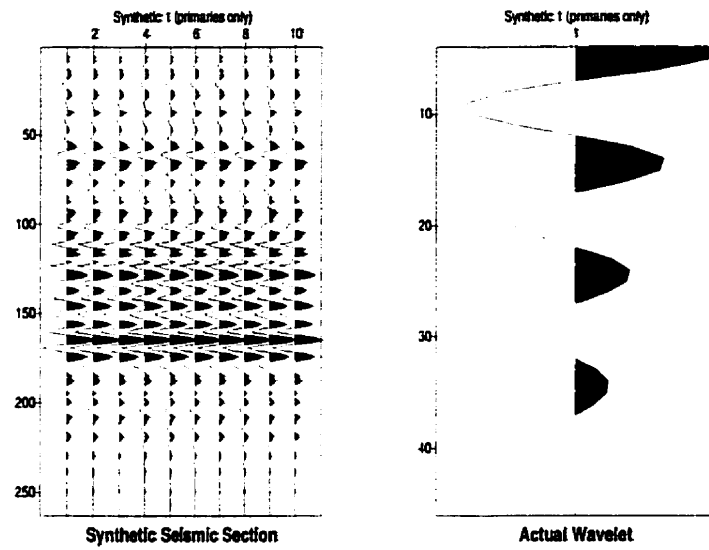


Figure 3.3: A primaries only minimum-phase synthetic trace and the model wavelet.

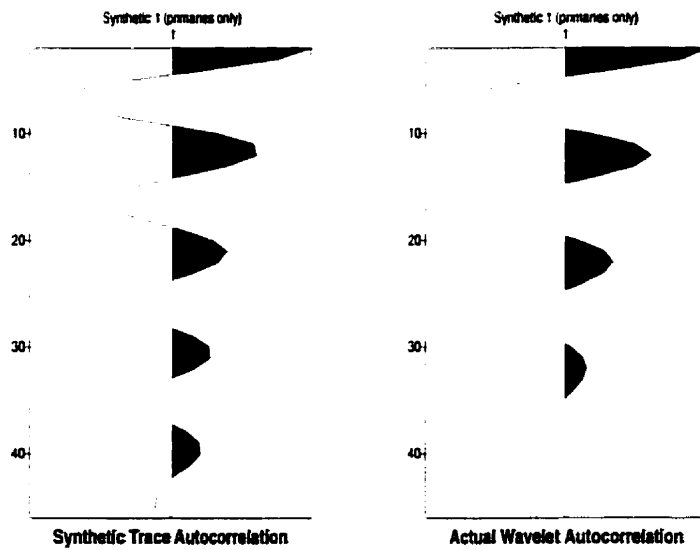


Figure 3.4: The trace autocorrelation and the model wavelet autocorrelation.

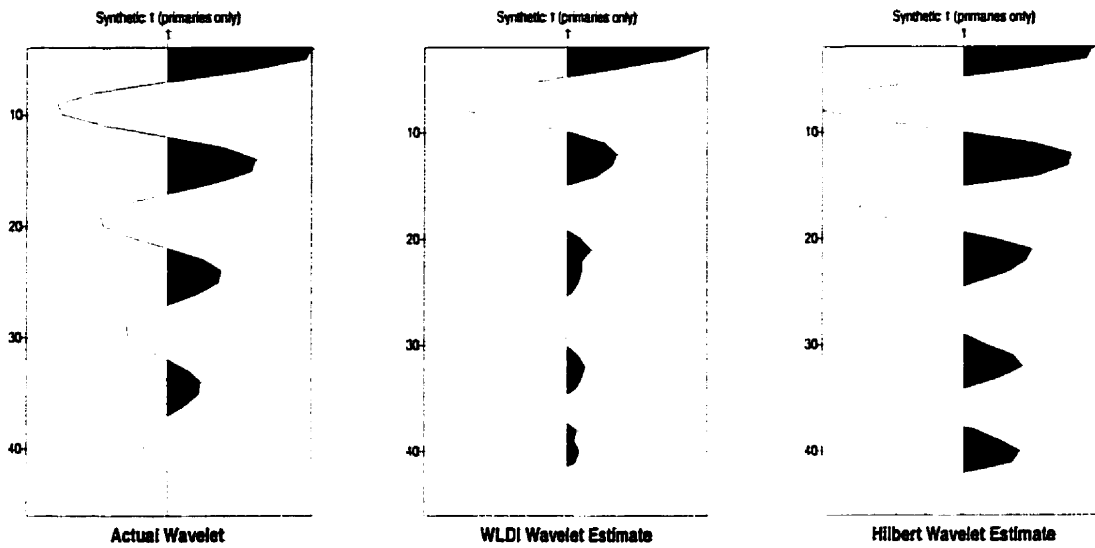


Figure 3.5: The model wavelet, a Wiener–Levinson double inverse (WLDI) estimate of the wavelet, and a Hilbert transform estimate of the wavelet.

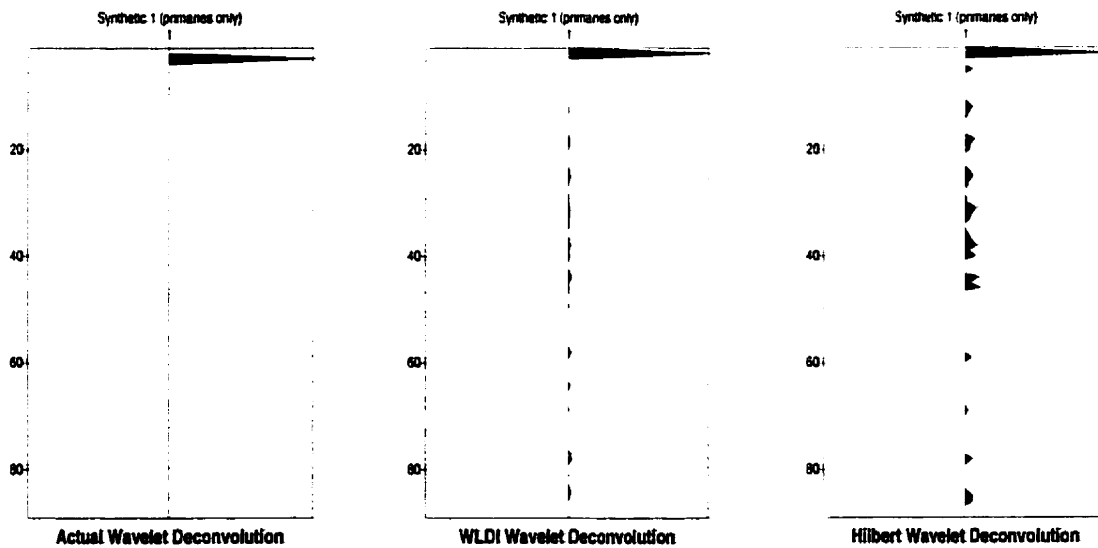


Figure 3.6: Model, Wiener–Levinson, and Hilbert wavelet deconvolutions.

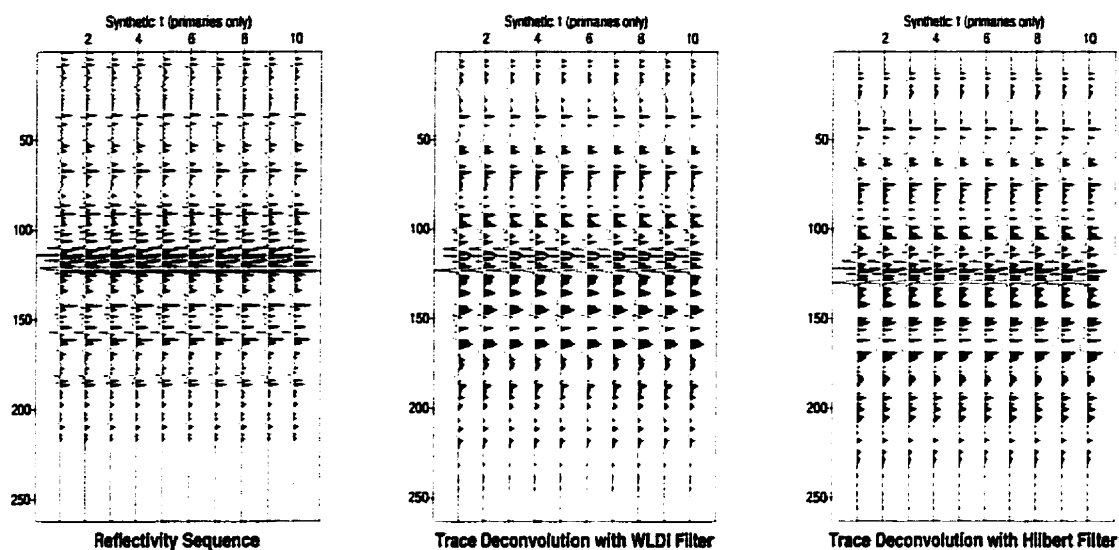


Figure 3.7: The actual well-log derived reflectivity series, the Wiener-Levinson reflectivity series estimate, and the Hilbert transform reflectivity series estimate.

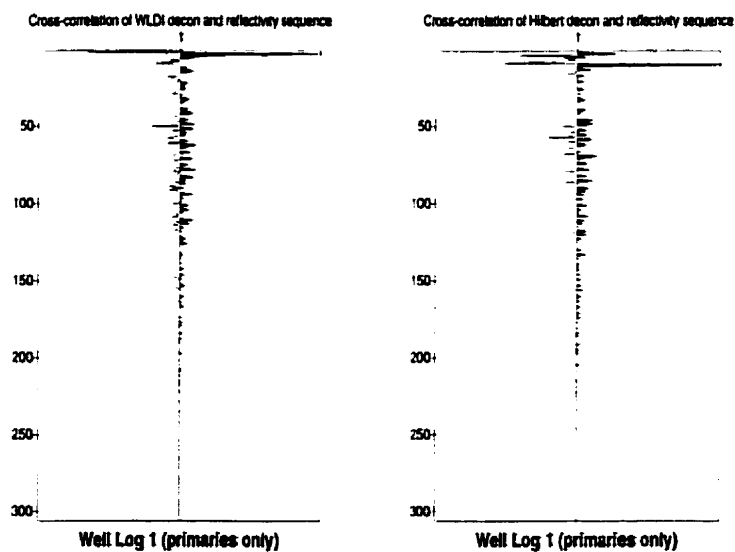


Figure 3.8: Cross-correlation of the actual reflectivity series with the Wiener-Levinson reflectivity series and the Hilbert transform reflectivity series.

### 3.3 Impulse response minimum phase synthetic data

Now the same analysis is conducted for a synthetic seismogram that contains multiples. This section is created in the same manner as above but multiples have been added by the method outlined by Robinson (1967). The inclusion of multiples in a synthetic seismic section generally worsens the whiteness assumption. Again, as an initial test, the trace and wavelet autocorrelations are compared (Figure 3.10). There is no significant difference between the two except that the trace autocorrelation seems to have the onset of a doublet near its end. The very close similarity between the trace and wavelet autocorrelations lends further support to the validity of the randomness assumption. Figure 3.11 shows the Wiener-Levinson and Hilbert transform estimates based on an input trace with multiples. Even though the whiteness assumption is worsened with multiples in the section, the resolving kernels (Figure 3.12) for the estimated wavelets are very good approximations to the expected spike response. The final 2 plots concerning this seismic section relate to the reflectivity sequence. Figure 3.13 compares the actual reflectivity to the estimated sequences. These estimated reflectivity sequences are quite good reproductions of the actual reflectivity. Once again, the estimated results are a bit smeared, due to the band limited nature of the seismic data, but there is no delay present. This causes events at 50, between 50 and 100, and at 150 on the actual sequence to correlate better to the same events on the estimated sequences. As above, the final image shown here is a comparison of cross-correlations. Both of these are very reasonable to the ideal result of a spike.

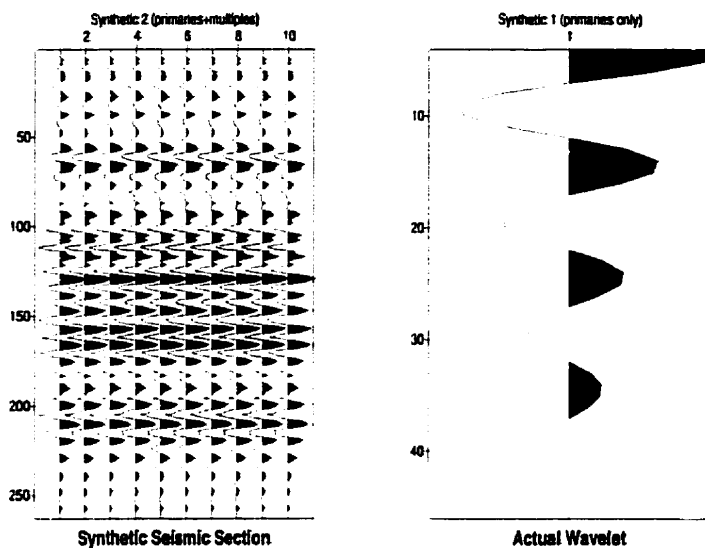


Figure 3.9: A primaries with multiples minimum-phase synthetic trace and the model wavelet.

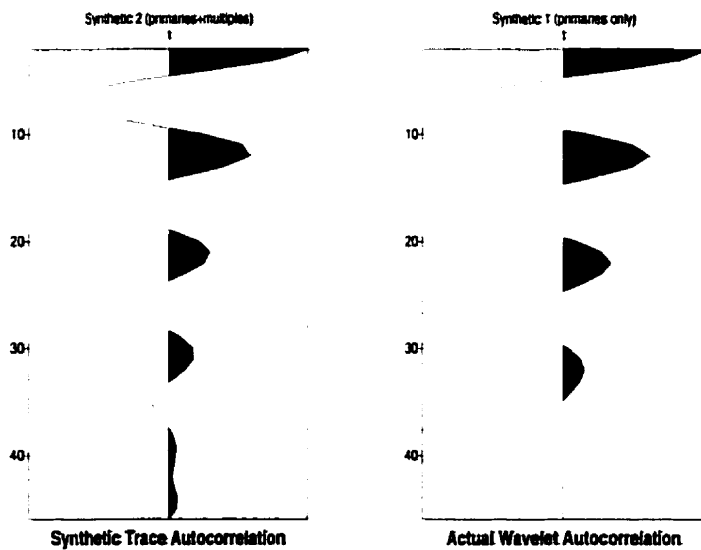


Figure 3.10: The trace autocorrelation and the model wavelet autocorrelation.

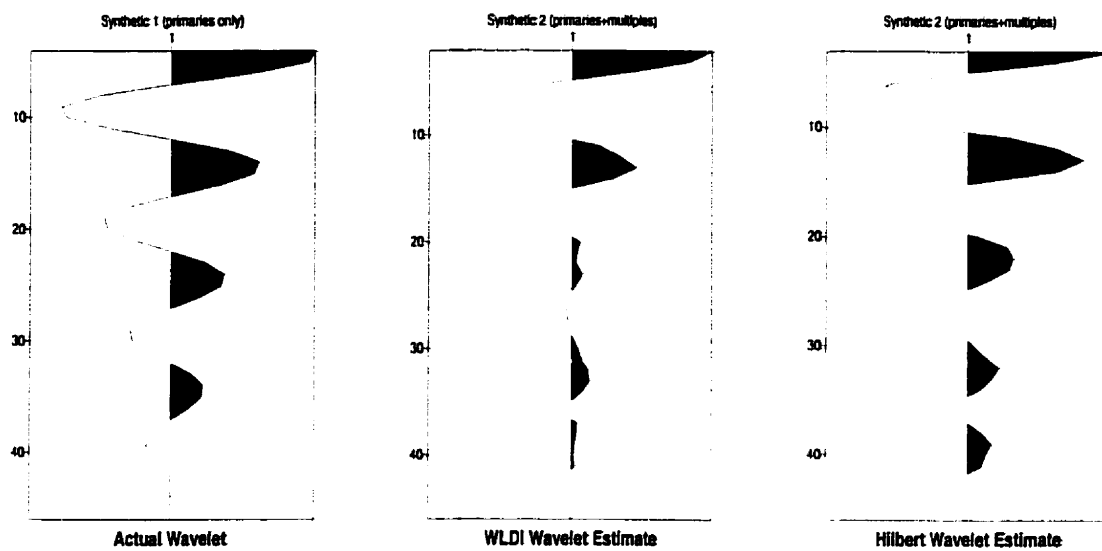


Figure 3.11: The model wavelet, a Wiener–Levinson double inverse (WLDI) estimate of the wavelet, and a Hilbert transform estimate of the wavelet.

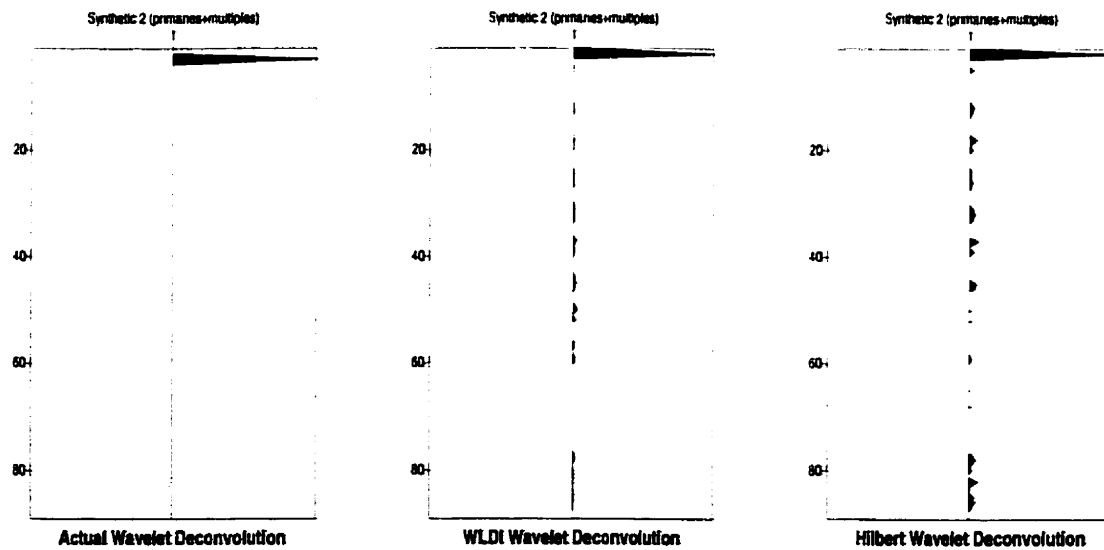


Figure 3.12: Model, Wiener–Levinson, and Hilbert wavelet deconvolutions.

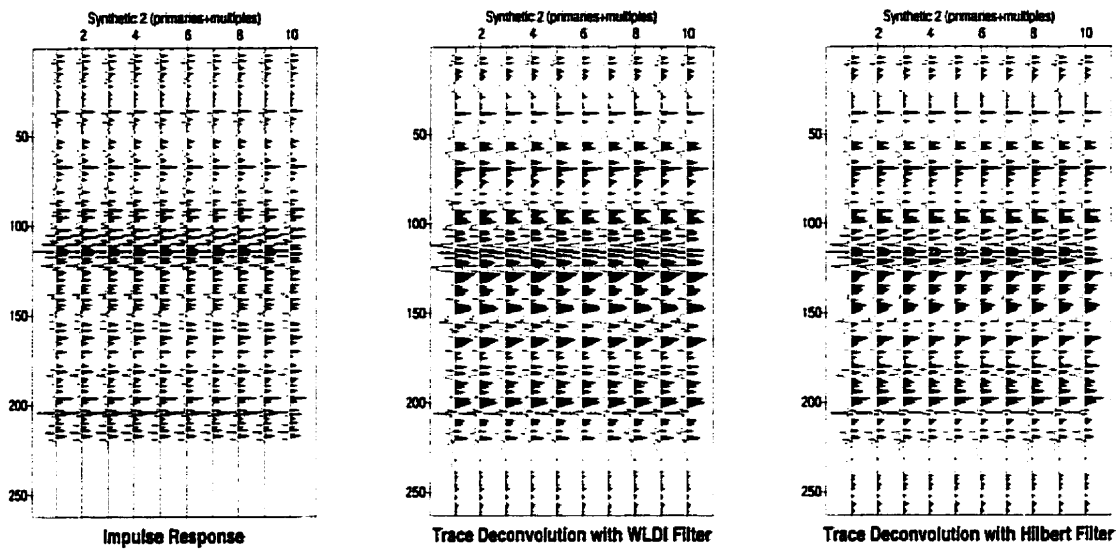


Figure 3.13: The actual well-log derived reflectivity series, the Wiener-Levinson reflectivity series estimate, and the Hilbert transform reflectivity series estimate.

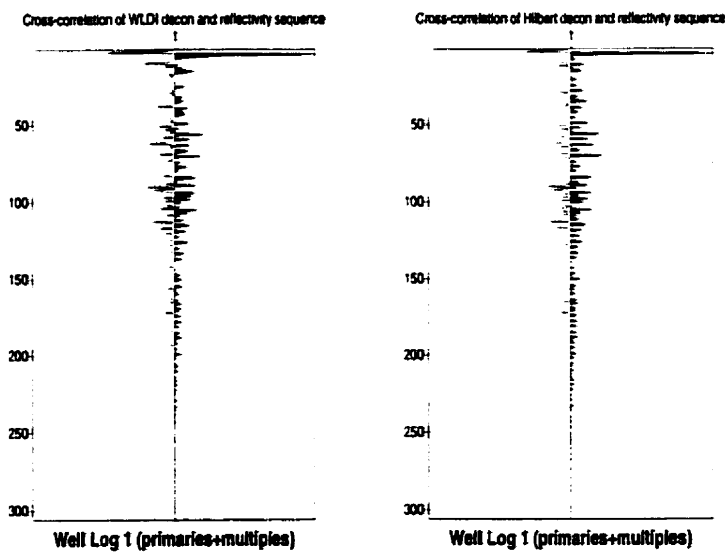


Figure 3.14: Cross-correlation of the actual reflectivity series with the Wiener-Levinson reflectivity series and the Hilbert transform reflectivity series.

### 3.4 Ideal zero phase synthetic data

Another common type of wavelet is the zero phase wavelet. When compared to minimum phase wavelets, these zero phase wavelets are symmetrical and are very broad band in the frequency domain. That being the case, an investigation into the changes that may occur when a zero phase wavelet is used in the reflectivity analysis is done. A zero phase Ricker wavelet that has a dominant frequency of  $30Hz$  is created to be the ideal model wavelet. Besides the fact that a zero phase wavelet is being used as the model, nothing else has changed and the analysis proceeds as before. The figures shown in this section concern investigations for a primaries only zero phase synthetic while those in the following section show results for a zero phase synthetic that contains primary and multiple arrivals.

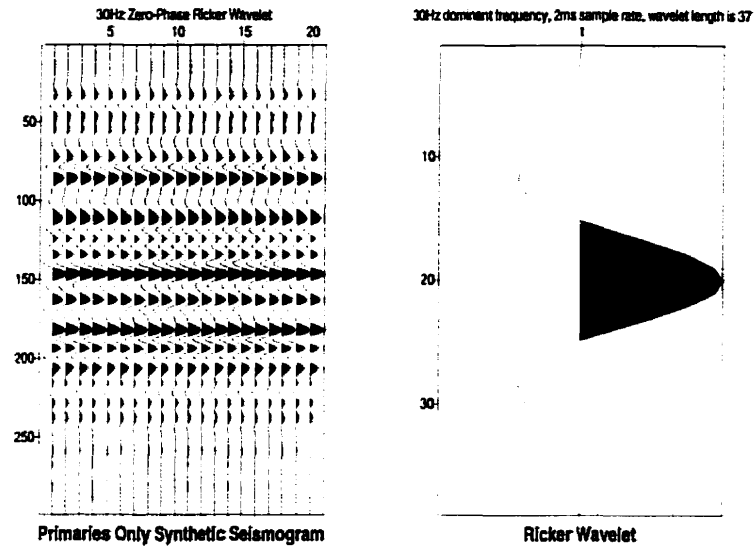


Figure 3.15: A primaries only zero-phase synthetic trace and the model Ricker wavelet.

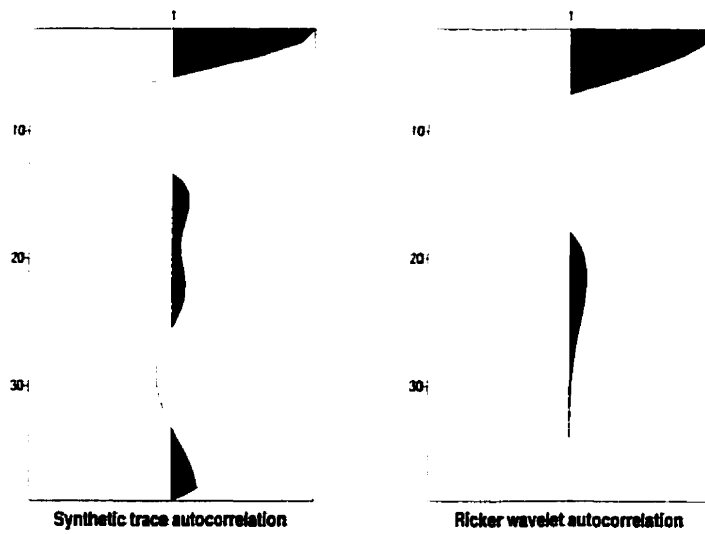


Figure 3.16: The trace autocorrelation and model Ricker wavelet autocorrelation.

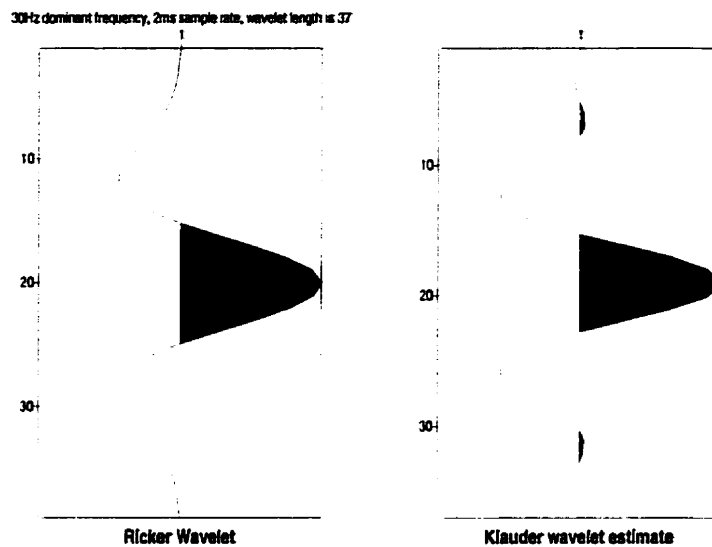


Figure 3.17: The model wavelet and a Klauder zero-phase estimate of the wavelet.

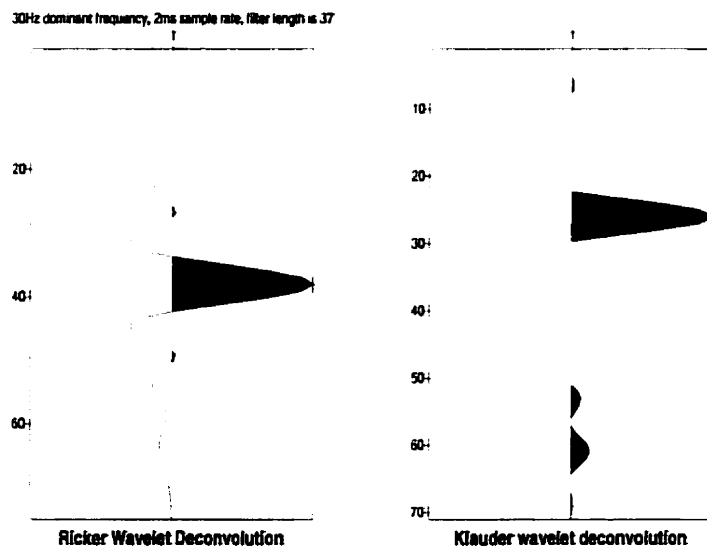


Figure 3.18: Ricker and Klauder wavelet deconvolutions.

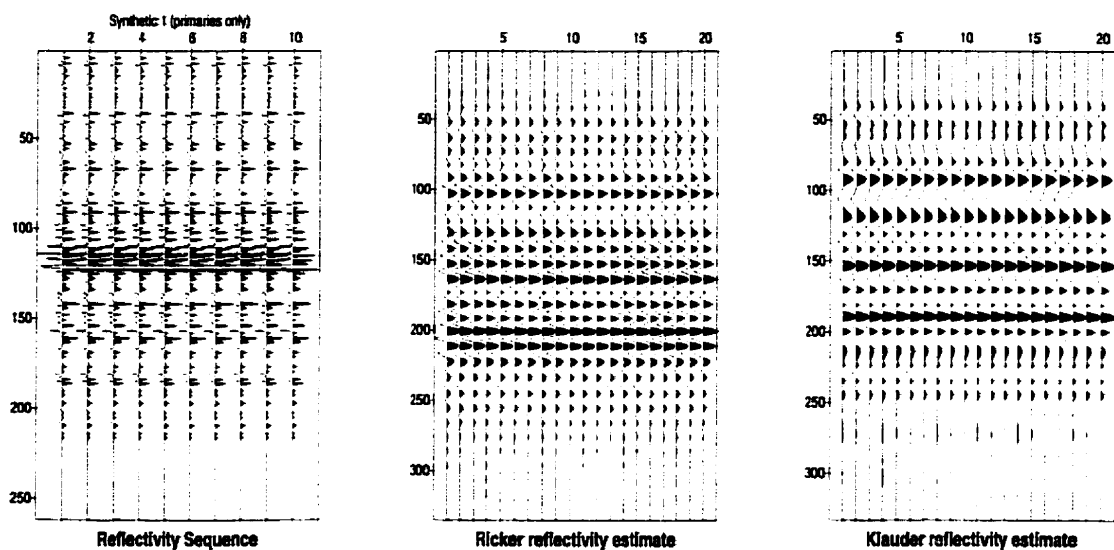


Figure 3.19: The actual well-log derived reflectivity series, the Ricker band limited reflectivity series estimate, and the Klaunder reflectivity series estimate.

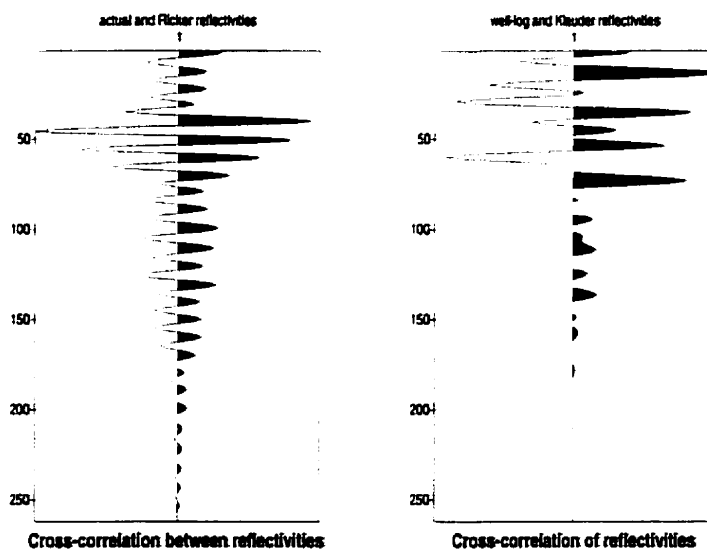


Figure 3.20: Cross-correlation of the actual reflectivity series with the Ricker band limited reflectivity series and the Klaunder reflectivity series.

### 3.5 Impulse response zero phase synthetic data

From Figures 3.15 – 3.26, note that the general trends discussed previously continue. Notice, in Figure 3.16 and Figure 3.22, that the trace autocorrelation and the wavelet autocorrelation are quite similar. Also note that the Klauder zero phase wavelet estimates, shown in Figures 3.17 and 3.23, are nearly identical to the model Ricker wavelet. Despite these similarities, some points of discussion arise. Figure 3.18 shows, for the 1<sup>st</sup> zero phase synthetic, that the Klauder and Ricker wavelet deconvolutions spike at different positions. Namely, the Klauder wavelet deconvolution has a spike that lags behind the spike seen for the Ricker wavelet. This lag is also evident in Figure 3.19, where the band limited reflectivity estimates are compared. It shows that events on the Klauder reflectivity sequence lag behind events on the Ricker reflectivity sequence. Figure 3.23 illustrates the close correlation between the Ricker wavelet and the Klauder estimate based on the zero phase synthetic with multiples. Their deconvolutions (Figure 3.24) spike at the same positions and are effectively identical. This similarity is also reflected in Figure 3.25. Here, the band limited reflectivities are shown and they too are effectively identical.

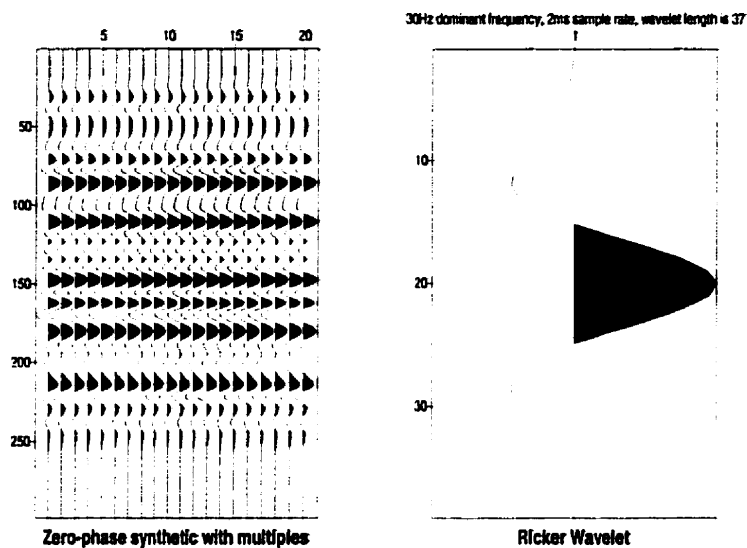


Figure 3.21: A primary with multiples zero-phase synthetic section and the model Ricker wavelet used to create it.

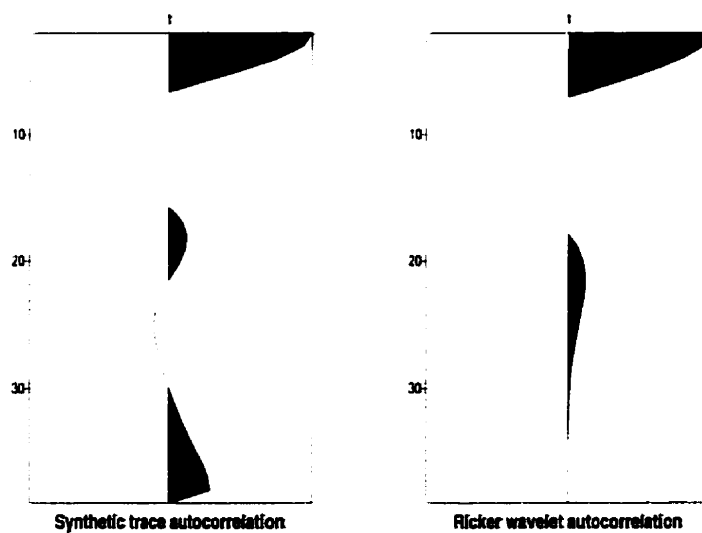


Figure 3.22: The trace autocorrelation and the Ricker wavelet autocorrelation.

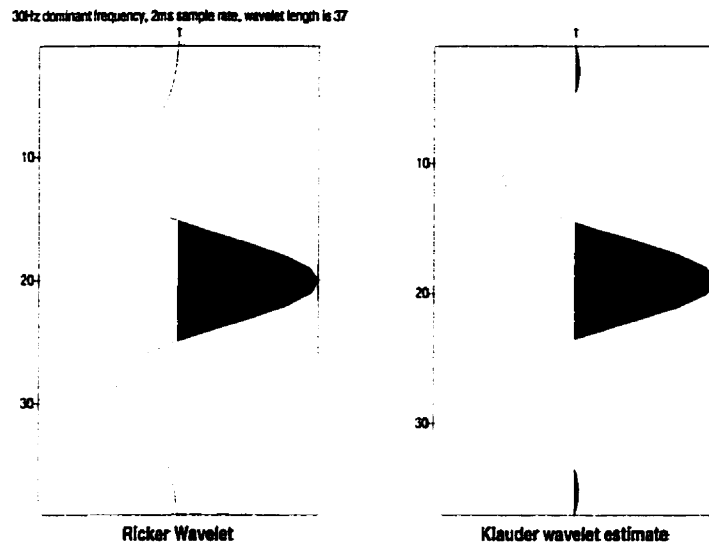


Figure 3.23: The model wavelet and a Klauder zero-phase estimate of the wavelet.

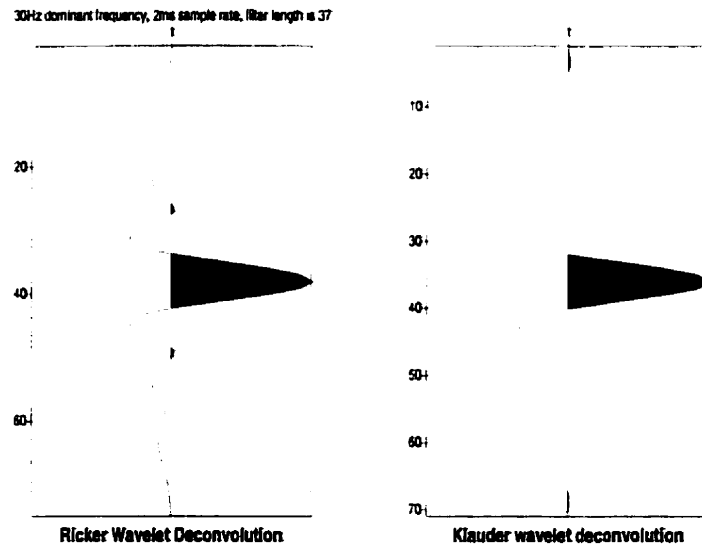


Figure 3.24: Ricker and Klauder wavelet deconvolutions.

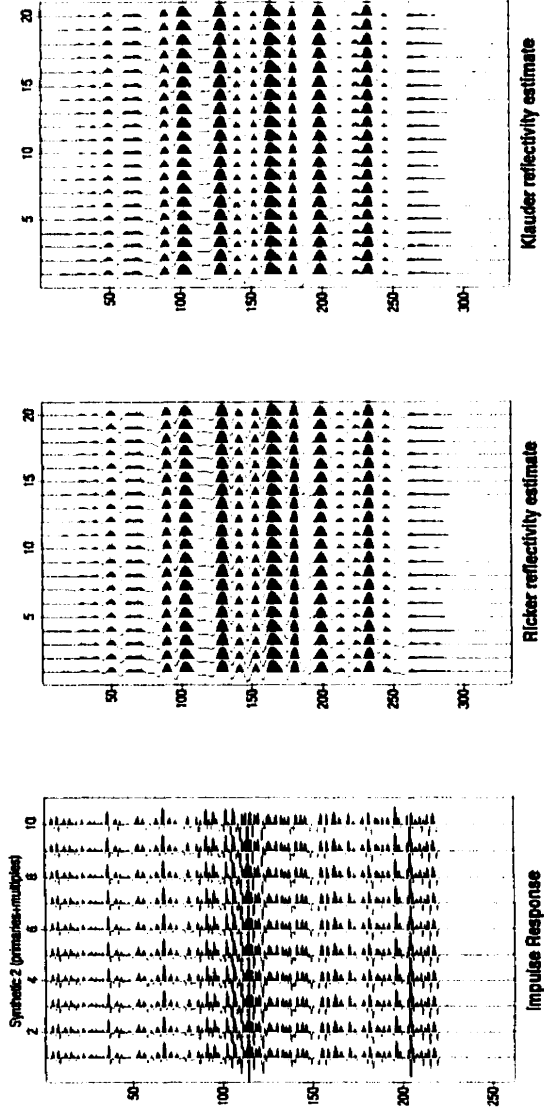


Figure 3.25: The actual well-log derived reflectivity series, the Ricker band limited reflectivity series estimate, and the Klauder reflectivity series estimate.

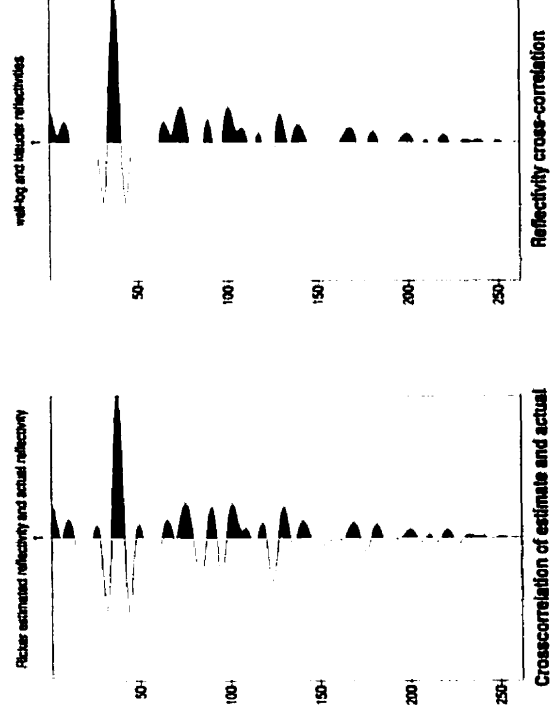


Figure 3.26: Cross-correlation of the actual reflectivity series with the Ricker reflectivity series and the Klauder reflectivity series.

### 3.6 Integration of VSP data with Vibroseis data

With the battery of tests on synthetic data concluded, the focus is now turned to an analysis on a real data set. The data set comes to CREWES through a gracious donation from PanCanadian Petroleum and is from a field in Alberta, Canada. Shown in Figure 3.27 is a near offset surface recording of real data shot with a vibroseis source and the down going vertical seismic profile (VSP) waveform. The VSP is also shot with a vibroseis source and it is this down going VSP waveform that is the in-situ measured wavelet. It, the in-situ wavelet, is a direct recording of the transmission energy. One thing to note about the waveform is that it, apparently, is illustrating a time varying nature. This violates the major assumption of the wavelet being stationary. Shown in Figure 3.28 is the autocorrelation of the reflected wave surface trace and the autocorrelation of the total down going VSP. The close similarity between the autocorrelations lends support to the assumption of a random reflectivity sequence. The direct measured wavelet is truncated to the same number of samples as a zero phase wavelet estimate. This gives a measured wavelet with a more reasonable length. A comparison of the two is shown in Figure 3.29. When plotted on the same scale, noticeable differences exist between the measured wavelet and the Klauder zero phase wavelet estimate. The most pronounced of these differences are in wavelet phase. It appears that the estimated wavelet is about 180 out of phase from the in-situ wavelet. This means that whenever there is a trough in the measured wavelet, there is a peak in the estimate. Also note what can be best described as difference in symmetry. What is meant by this is that the estimate is a typical zero phase wavelet in that it is symmetric about its major peak. However, this is not what is seen in the truncated measured wavelet. There is

no symmetry about the major trough. In fact, it appears as if the in-situ measurement is a delayed minimum phase wavelet of sorts. Although there are these significant differences between the two, the autocorrelation of the real seismic trace data is quite similar to the autocorrelations of the truncated and estimated wavelets (see Figure 3.30). The wavelet autocorrelations themselves are also quite similar to each other. Collectively, this reinforces the belief that trace and wavelet autocorrelations are approximations of each other and, hence, the reflectivity is random. Resolving kernels for the deconvolution of the different wavelets (in-situ, in-situ truncated, and statistical zero phase) are shown in Figure 3.31. All three give good, relatively clean, spikes but the spikes all occur at different positions. These different spiking positions may imply that the phase differences and nonstationarity of the wavelet itself are important. That is, the different spiking positions may be due to different phases and the nonstationary nature of the wavelet. The final figure, Figure 3.32, relates to how well the deconvolution filters work. Since there is no well log derived reflectivity sequence to act as a control for the results, we proceed in a slightly different manner. Instead of comparing estimated sequences to the actual sequence, we evaluate the results with respect to how well responses are brought out and if the ringy nature of the surface data can be suppressed. Note that the deconvolution result from a filter based on the Klauder zero phase wavelet estimate best reduces the ringiness and responses are very clear.

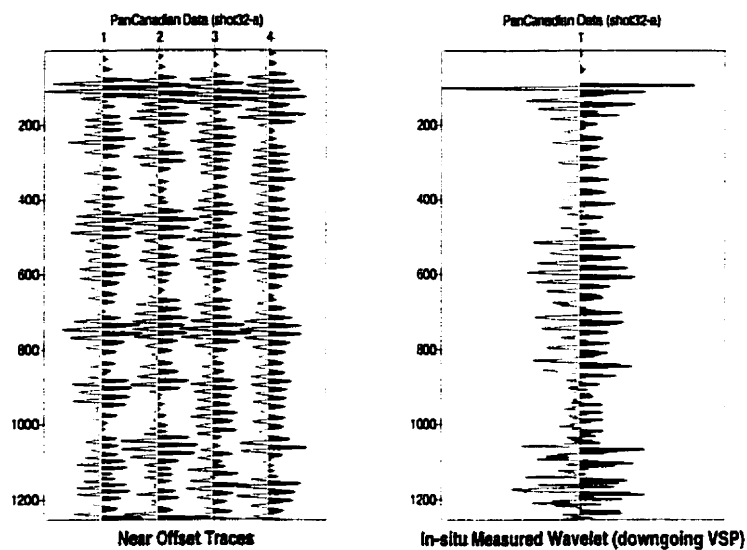


Figure 3.27: Near offset surface data and the in-situ measured wavelet (down going VSP)

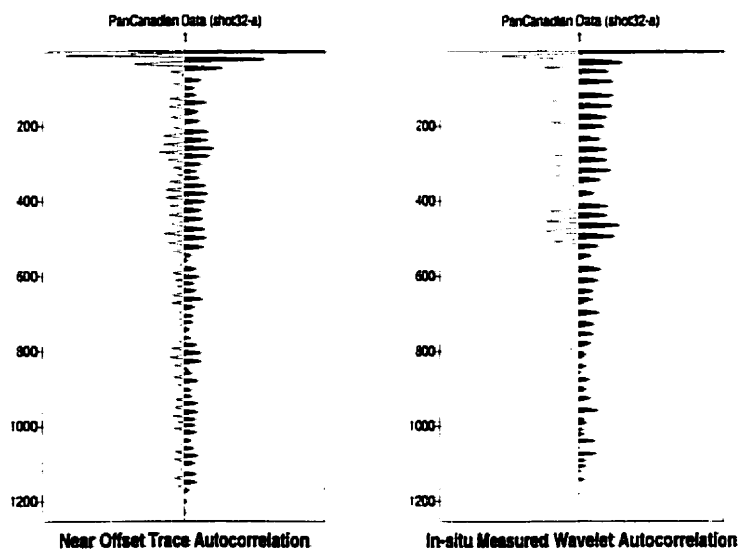


Figure 3.28: Near offset trace autocorrelation and in-situ wavelet autocorrelation

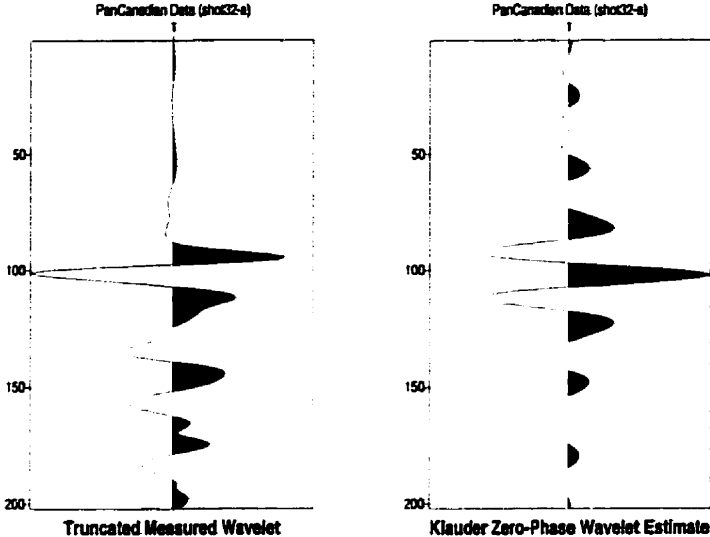


Figure 3.29: Truncated measured wavelet and a Klauder zero-phase wavelet.

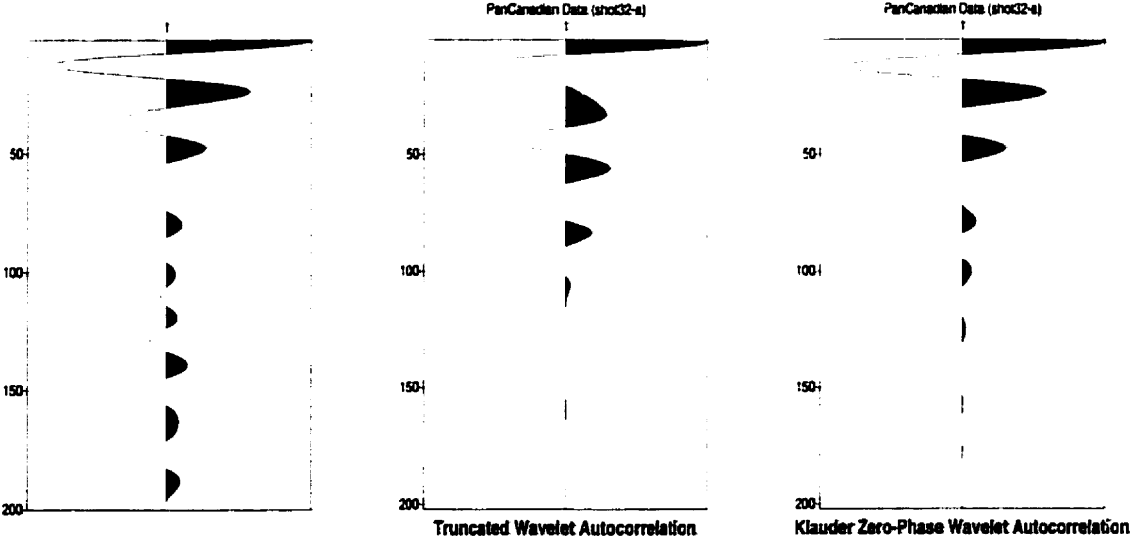


Figure 3.30: Near offset trace autocorrelation, truncated wavelet autocorrelation, and Klauder wavelet autocorrelation.

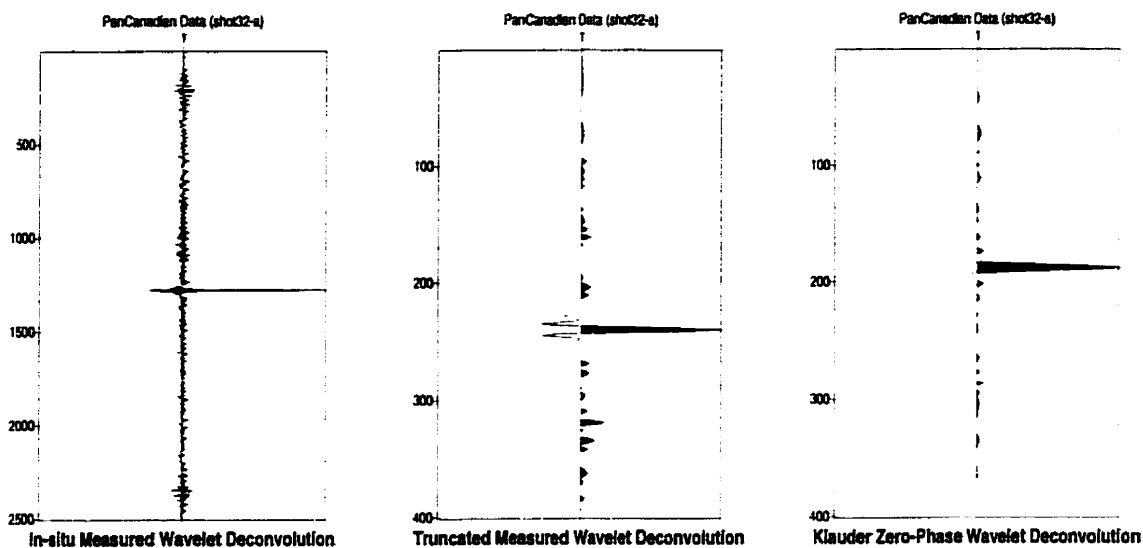


Figure 3.31: Measured wavelet deconvolution, truncated wavelet deconvolution, and Klauder wavelet deconvolution.

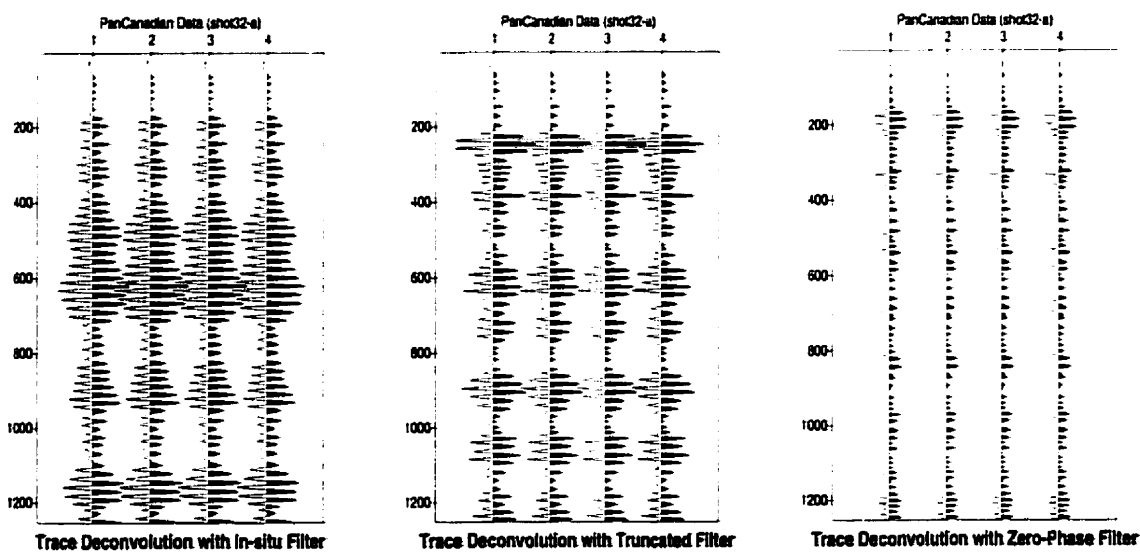


Figure 3.32: Near offset traces and their convolution with an in-situ, truncated, and Klauder filter.

# Chapter 4

## The phase assumption

### 4.1 Proposed tests for the phase assumption

An extensive analysis of the phase assumption made in statistical deconvolution has led to the development of two tests for phase. The first test to check the validity of the phase assumption is fairly simple and easy to apply. It assumes that a trace and a wavelet (measured or estimated) exists. From this trace, a deconvolution filter is estimated based on the seismic trace. As in the previous case of the randomness test, the design of the deconvolution filter is based on the seismic trace since this is what is generally available in the case of real data. Then, the actual wavelet is convolved with the estimated filter to produce a resolving kernel which is compared to the ideal spiking response. The resolving kernels similarity to a spike will dictate the goodness of the phase assumption being made. A pseudocode describing this test is outlined below. The second test involves a well-log derived reflectivity sequence. Statistically estimated minimum phase wavelets are created from the input trace. These wavelets are then used to estimate minimum phase deconvolution filters.

The filters are convolved with the input trace to generate reflectivity estimates. Comparisons of these estimates to the well-log derived reflectivity will allow one to ascertain the goodness of the phase assumption being made. Again, the flow charts that outline these tests (shown below) are followed by the pseudocode for the tests themselves.

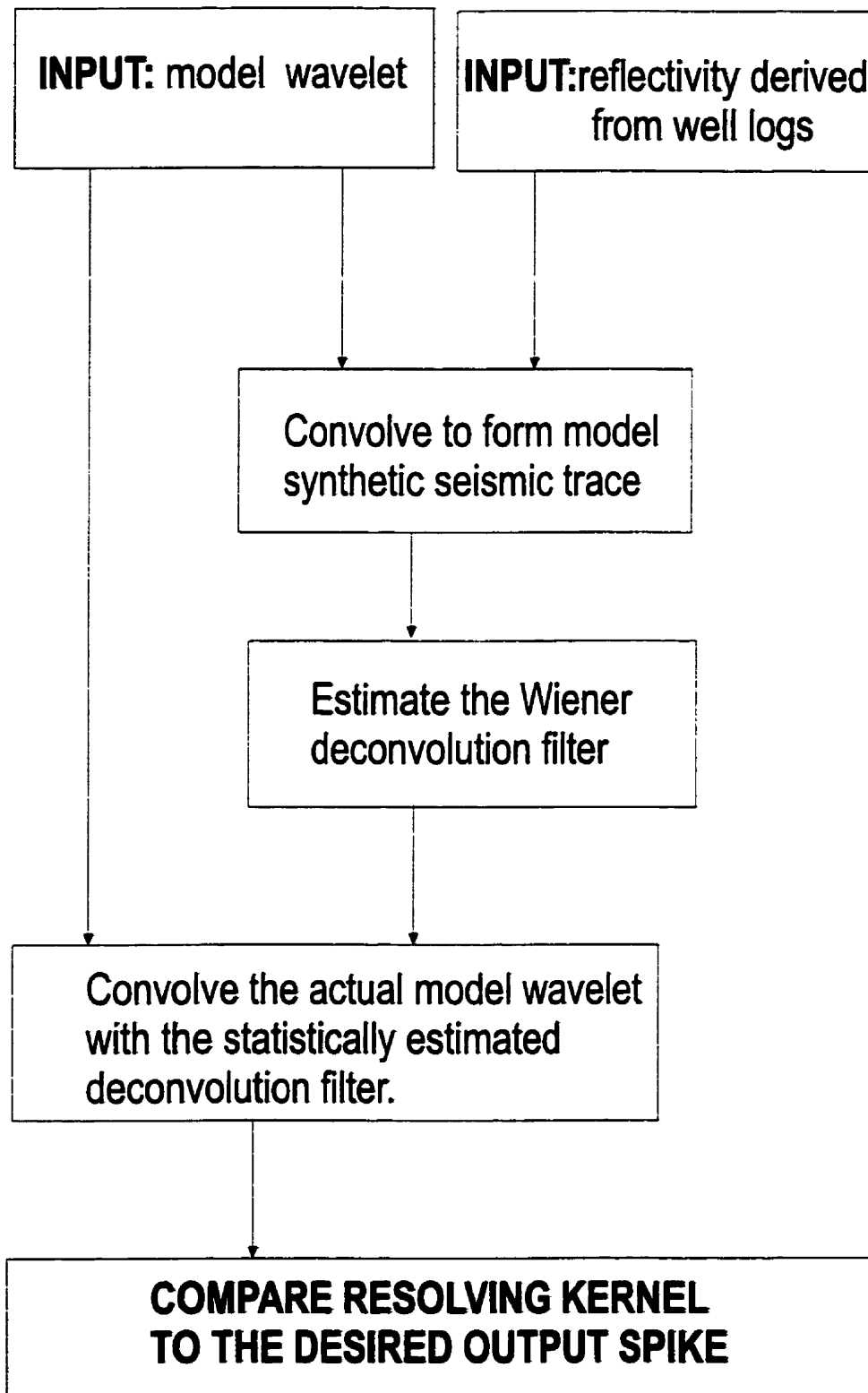


Figure 4.1: A validity test of wavelet phase assumption.

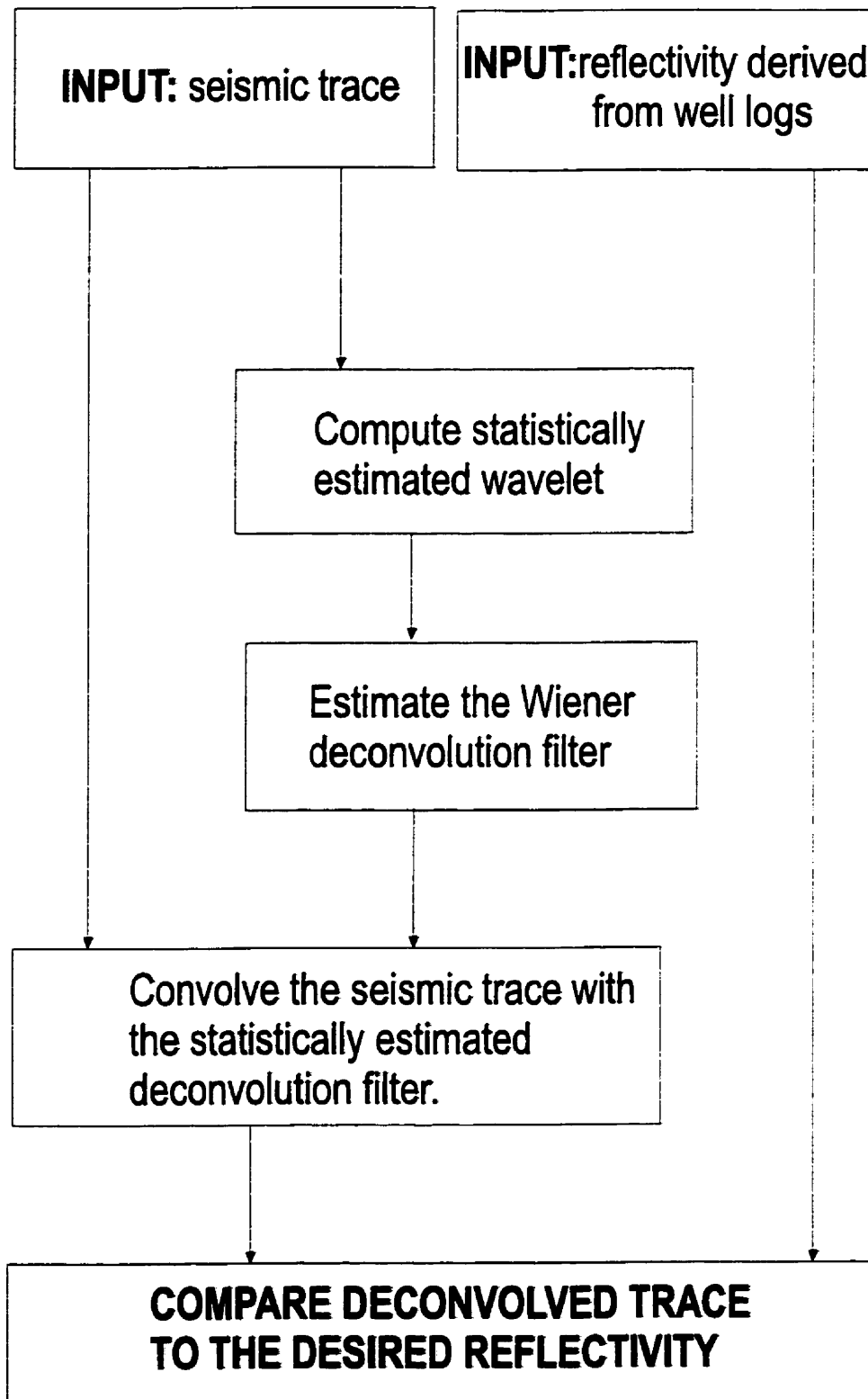


Figure 4.2: A well-log validity test of wavelet phase assumption.

**BEGIN:** A validity test for the minimum phase assumption.

**for each seismic trace do**

*compute statistical estimate of deconvolution filter  $f(n)$ , or  $\vec{f}$ ,*

*using the Wiener–Levinson method;*

*compute the resolving kernel;*

*compare to the desired output delta function **end do***

**where**

**proc**  $\vec{f} = \mathbf{R}^{-1}\vec{g}$ ,  $\mathbf{R}$  is the autocorrelation matrix of the input trace  $s(n)$ ;

**proc** resolving kernel  $\equiv \forall n|n \geq 0, w(n) * f(n) = \sum_{\tau=0}^{\tau=N} w(\tau)f(n - \tau)$ ,

*$w(n)$  is the actual wavelet being considered.*

**END**

**BEGIN:** A well–log validity test for the minimum phase assumption.

**for each seismic section do**

*compute desired statistically estimated wavelet  $w(n)$ , or  $\vec{w}$ ;*

*compute deconvolution filter  $f(n)$ , or  $\vec{f}$ , based on said wavelet;*

*compute the trace deconvolution;*

*compare to the well–log derived reflectivity sequence **end do***

**where**

**proc**  $\vec{w} = (\mathbf{R}^{-1}\vec{g})^{-1}$ ,  $\mathbf{R}$  is the autocorrelation matrix of the trace  $s(n)$ ;

**proc**  $\vec{f} = \mathbf{W}^{-1}\vec{g}$ ,  $\mathbf{W}$  is the autocorrelation matrix of the wavelet;

**proc** trace deconvolution  $\equiv \forall n|n \geq 0, s(n) * f(n) = \sum_{\tau=0}^{\tau=N} s(\tau)f(n - \tau)$ .

**END**

These tests will be used on two model environments. Each of these models have a minimum delay wavelet, two mixed delay wavelets, and a maximum delay wavelet, as well as their corresponding synthetic traces. The remaining sections of this chapter present the model environments and a comprehensive set of results regarding the investigations on the phase assumption with these models.

### 4.1.1 model 1

Presented here and in the following subsection are the two model environments where the minimum phase assumption is investigated. Each of these scenarios incorporates a minimum delay wavelet, an end-loaded mixed delay wavelet, a front-loaded mixed delay wavelet, and a maximum delay wavelet. An end-loaded mixed delay wavelet refers to a mixed delay wavelet whose energy is concentrated closer to its end. A front-loaded mixed delay wavelet refers to a mixed delay wavelet whose energy is maximally concentrated at its onset. These models also contain the synthetic traces associated with each of wavelets and the reflectivity sequence used to create the synthetics. In addition, the minimum delay synthetic is used to generate two statistical minimum delay wavelet estimates and their deconvolution filters. The trace deconvolution investigations use these statistically estimated filters.

Figures 4.3 – 4.6 show the various wavelets used in this model, the common reflectivity sequence for the model, and the associated synthetic traces. Note that the reflectivity is a primaries only reflectivity sequence (i.e. no multiples) and is convolved with each of wavelets to give the traces shown to the right. The mixed delay wavelet in Figure 4.4 is end-loaded, while in Figure 4.5 is a front-loaded mixed delay wavelet. The final two images shown (Figures 4.7 and 4.8) are the statistically estimated minimum delay wavelets. Figure 4.7 shows the model minimum delay wavelet, a Hilbert transform wavelet estimate, and the deconvolution filter associated with it. This figure shows that the model wavelet and the Hilbert transform estimate are similar waveforms but have different time delays and the statistical estimate has some minor noise in its tail. Figure 4.8 also shows the model minimum delay wavelet but the statistical wavelet and its filter are generated by the Wiener-Levinson

method. Here, the waveforms are very dissimilar. In particular, the Wiener–Levinson double inverse wavelet is quite front-loaded with minimal amounts of tail energy and is extremely characteristic of a spike response.

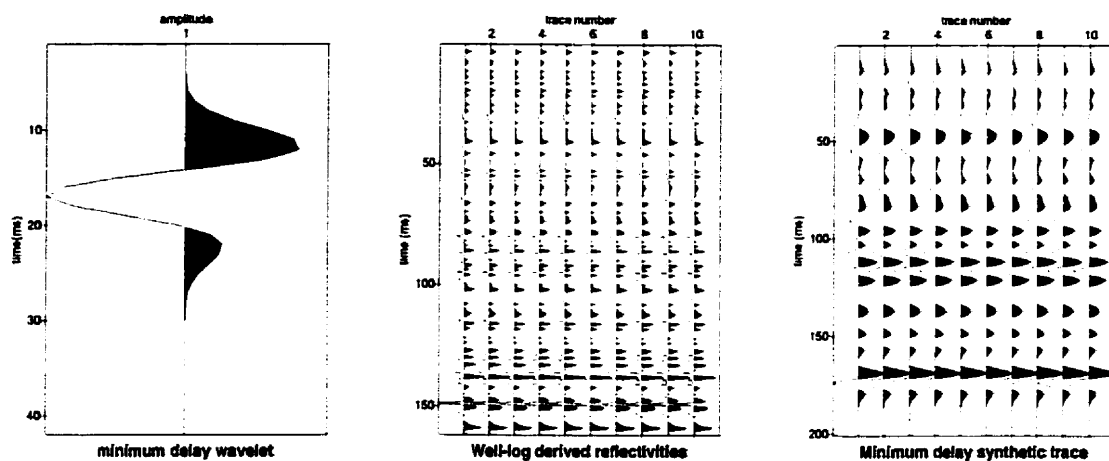


Figure 4.3: The minimum delay wavelet,  $(-1.1 + z)^2(1.75 + z)^{38}$ , and primaries only reflectivity sequence are convolved to give the synthetic trace to the right.

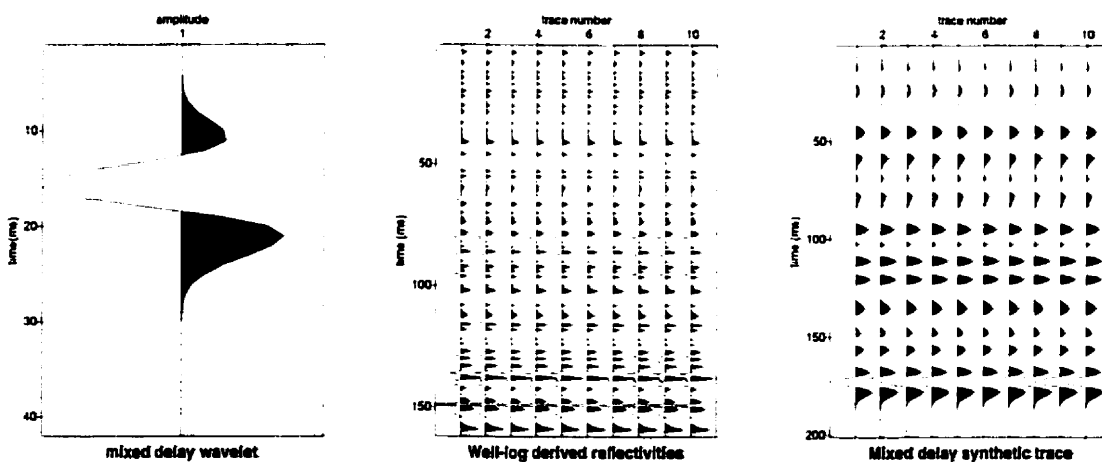


Figure 4.4: A mixed delay wavelet,  $(1 - 1.1z)^2(1.75 + z)^{38}$ , and a primaries only reflectivity sequence are convolved to give the synthetic trace to the right.

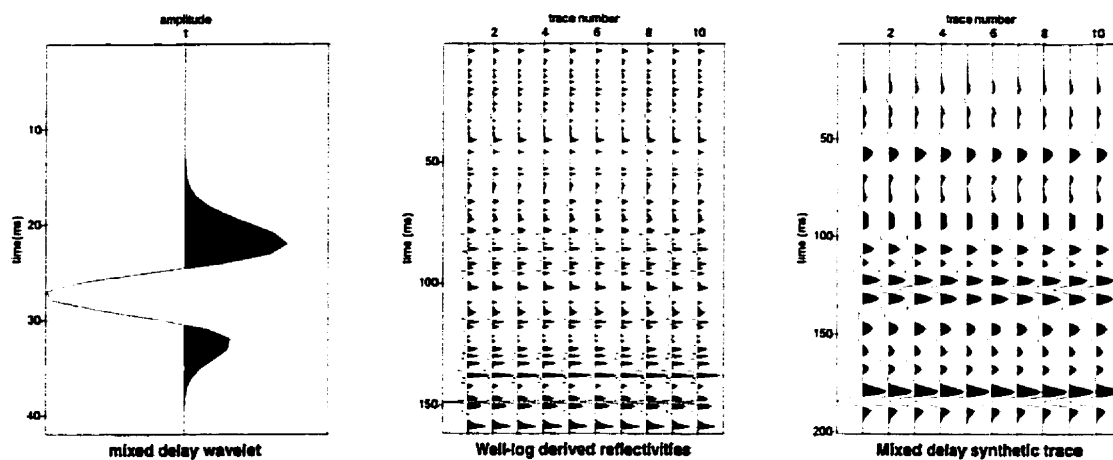


Figure 4.5: A mixed delay wavelet,  $(-1.1 + z)^2(1 + 1.75z)^{38}$ , and a primaries only reflectivity sequence are convolved to give the synthetic trace to the right.

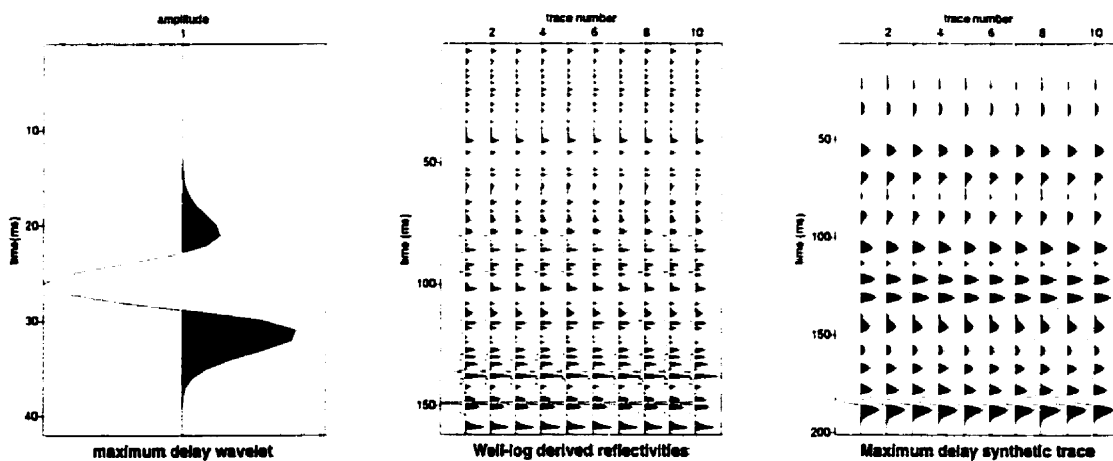


Figure 4.6: The maximum delay wavelet,  $(1 - 1.1z)^2(1 + 1.75z)^{38}$ , and primaries only reflectivity sequence are convolved to give the synthetic trace to the right.

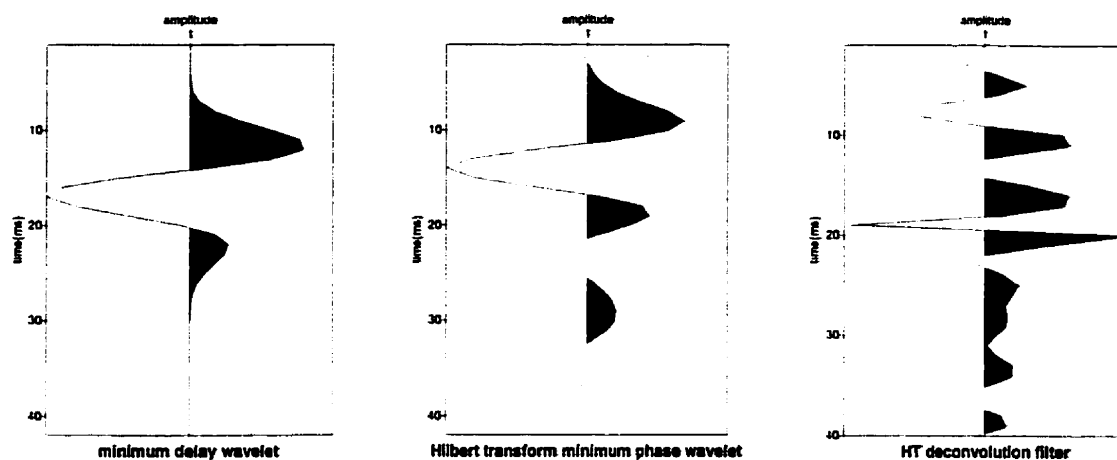


Figure 4.7: The actual minimum delay wavelet (left) for this model, the Hilbert transform minimum delay wavelet estimate (center) for this model and the deconvolution filter (right) estimated from it.

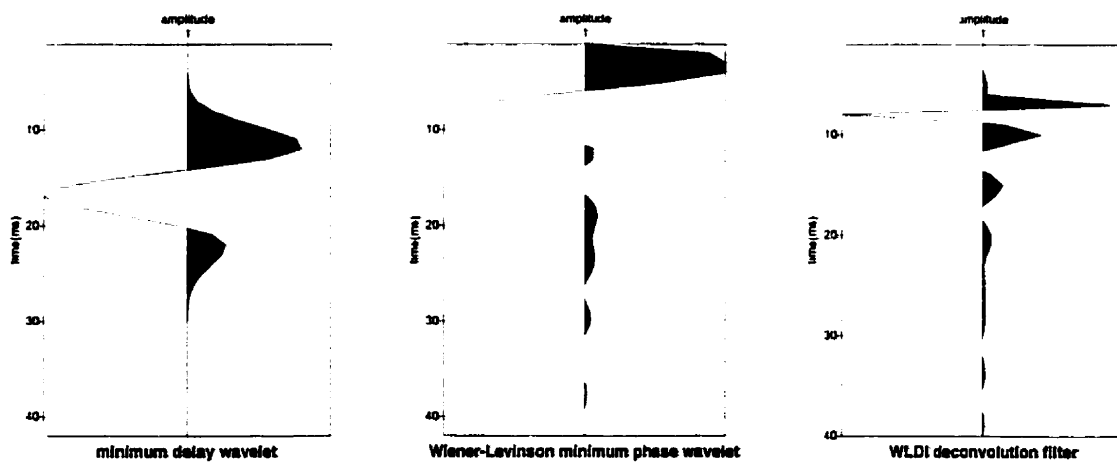


Figure 4.8: The the actual minimum delay wavelet (left) for this model, the Wiener-Levinson minimum delay wavelet estimate (center) for this model and the deconvolution filter (right) estimated from it.

## 4.1.2 model 2

Figures 4.9 – 4.14 show the various wavelets used in this model, the common reflectivity sequence for the model, and the associated synthetic traces. Note that the reflectivity is a primaries only reflectivity sequence (i.e. no multiples) and is convolved with each of wavelets to give the traces shown to the right. The mixed delay wavelet in Figure 4.10 is front-loaded, while in Figure 4.11 is an end-loaded mixed delay wavelet. Notice that all of the model wavelets used here have large band-widths and have very little energy distribution. That is, virtually all the energy is concentrated at the waveforms onset or at its end. The final two images shown for this subsection (Figures 4.13 and 4.14) are the statistically estimated minimum delay wavelets. Figure 4.13 shows the model minimum delay wavelet, a Hilbert transform wavelet estimate, and the deconvolution filter associated with it. This figure shows that the model wavelet and the Hilbert transform estimate are similar waveforms but have different time delays and the statistical estimate has some notable noise in its tail. Figure 4.14 also shows the model minimum delay wavelet but the statistical wavelet and its filter are generated by the Wiener-Levinson method. Here, the waveforms are very dissimilar. In particular, the Wiener-Levinson double inverse wavelet is quite front-loaded with minimal amounts of tail energy and is extremely characteristic of a spike response with large band-width.

Figure 4.10: A mixed delay wavelet,  $(1 - 1.35z)^2(1.5 + z)^{38}$ , and a primaries only reflectivity sequence are convolved to give the synthetic trace to the right.

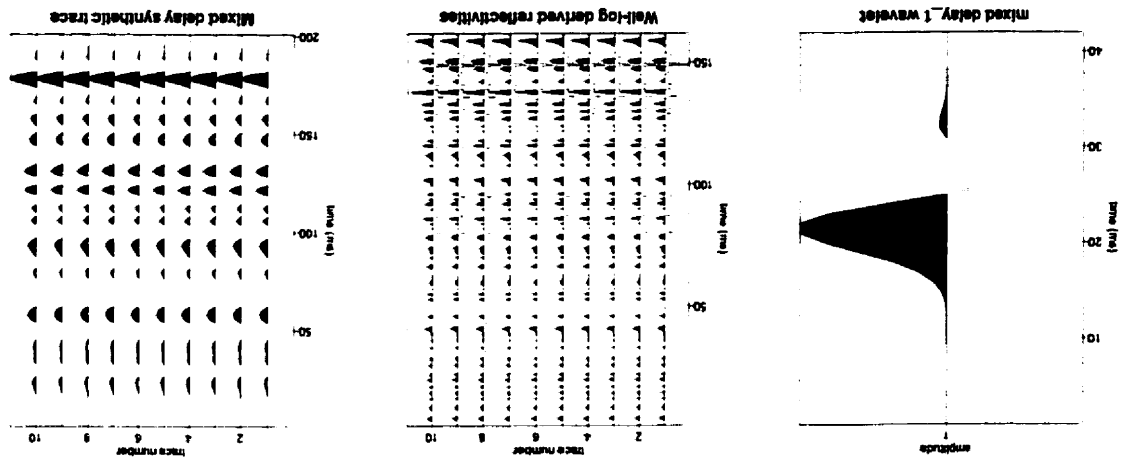
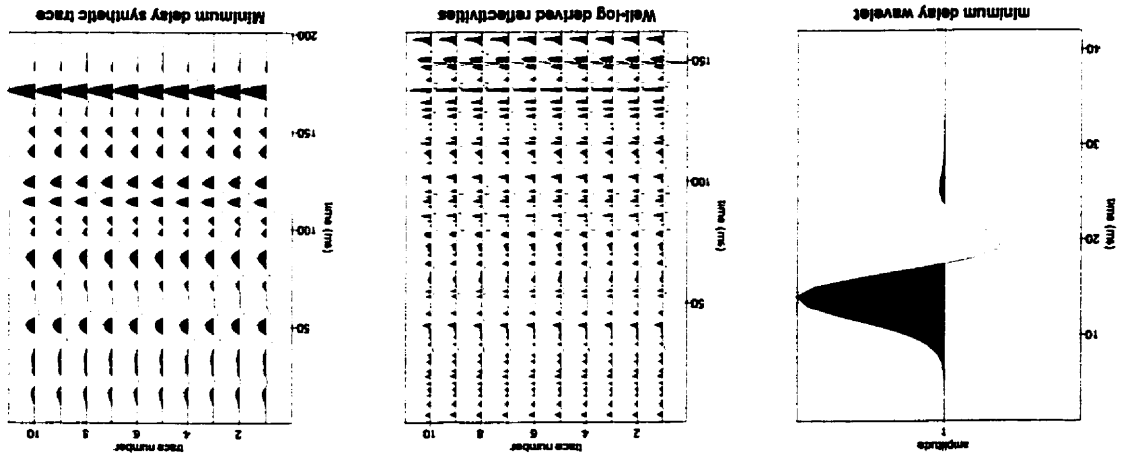


Figure 4.9: The minimum delay wavelet,  $(-1.35 + z)^2(1.5 + z)^{38}$ , and primaries only reflectivity sequence are convolved to give the synthetic trace to the right.



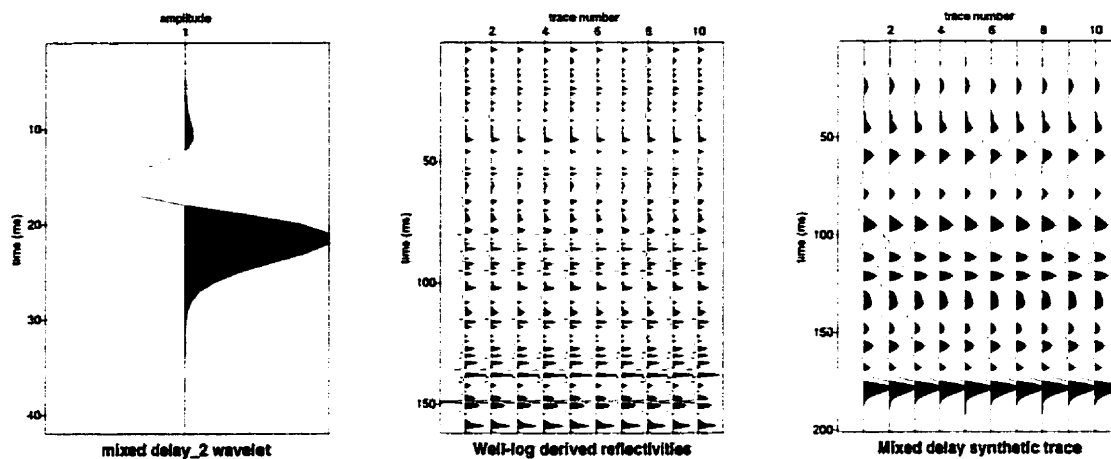


Figure 4.11: A mixed delay wavelet,  $(-1.35 + z)^2(1 + 1.5z)^{38}$ , and a primaries only reflectivity sequence are convolved to give the synthetic trace to the right.

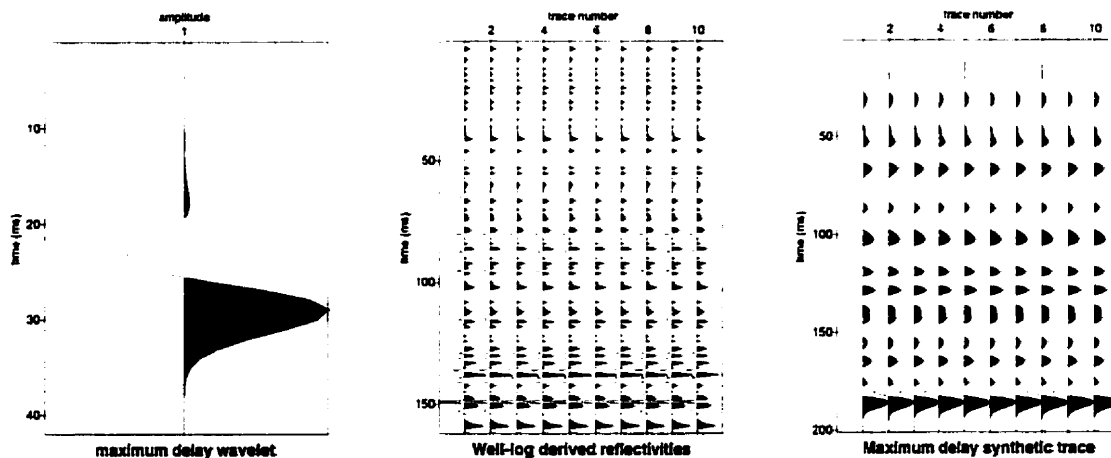


Figure 4.12: The maximum delay wavelet,  $(1 - 1.35z)^2(1 + 1.5z)^{38}$ , and primaries only reflectivity sequence are convolved to give the synthetic trace to the right.

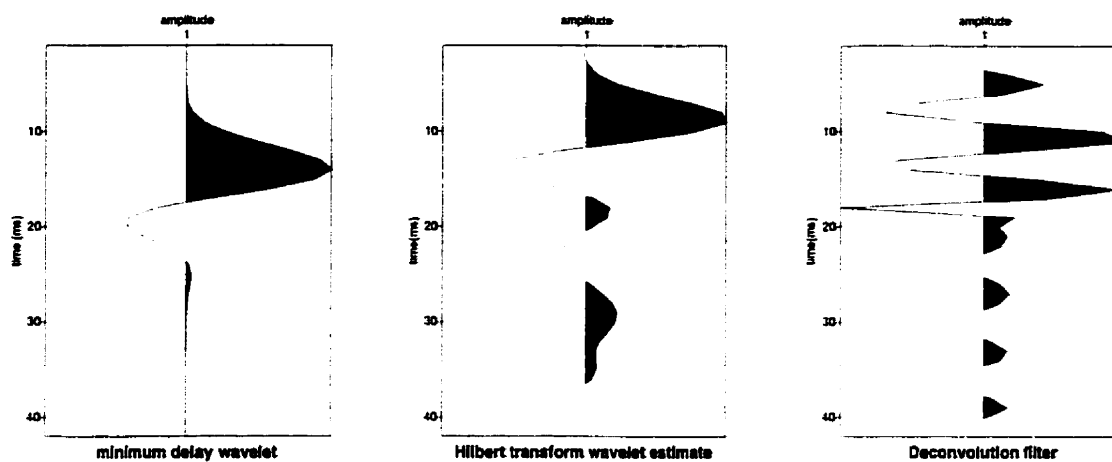


Figure 4.13: The actual minimum delay wavelet (left) for this model, the Hilbert transform minimum delay wavelet estimate (center) for this model and the deconvolution filter (right) estimated from it.

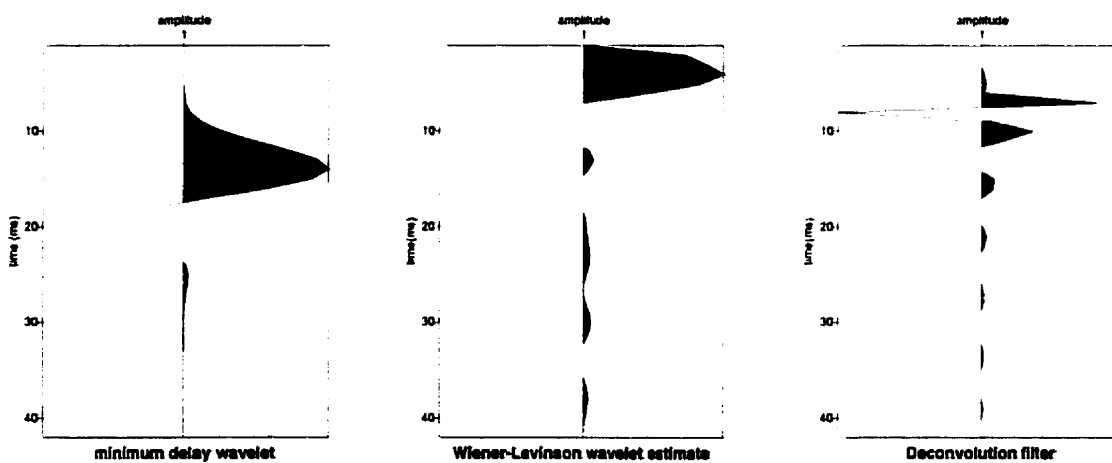


Figure 4.14: The actual minimum delay wavelet (left) for this model, the Wiener-Levinson minimum delay wavelet estimate (center) for this model and the deconvolution filter (right) estimated from it.

## 4.2 Phase effects on resolving kernels

### 4.2.1 results: model 1

Figures 4.15 through 4.18 show the resolving kernel tests for the first model minimum delay wavelet and its selected permutations. The minimum phase wavelet has the  $z$ -dipole form  $(-1.1 + z)^2(1.75 + z)^{38}$  and the permutations considered are:  $(1 - 1.1z)^2(1.75 + z)^{38}$  (mixed delay),  $(-1.1 + z)^2(1 + 1.75z)^{38}$  (mixed delay), and  $(1 - 1.1z)^2(1 + 1.75z)^{38}$  (maximum delay).

In Figure 4.15, a spiking deconvolution filter for the minimum delay wavelet is shown along with the wavelet itself and the resulting resolving kernel. The convolution of the Wiener deconvolution filter with the wavelet produces the resolving kernel shown in this figure. This is a sharp resolving kernel with a narrow band-width. The optimal spiking position is at  $25ms$  and there is insignificant energy in the tail of the kernel. If the dipoles for the 1<sup>st</sup> term are interchanged, the end-loaded mixed delay wavelet shown in Figure 4.16 results. The deconvolution, in this case, produces a resolving kernel which is almost identical to the minimum phase situation with the exception being that now the optimal spiking position is at  $44ms$ . Similarly, in Figure 4.17, the second mixed delay wavelet (front-loaded) has a sharp resolving kernel with narrow band-width and an optimum spiking position at  $36ms$ . Figure 4.18 shows the resolving kernel result for the maximum delay wavelet. In this case, the kernel is sharp with a spiking position at  $55ms$  but the kernel has a broader band-width than the previous three images. The general observed trend is that as the phase delay of the wavelet changes, so does the optimum spiking position. This is seen by comparing the optimum spiking positions of the various resolving kernels. In other words, if the wavelet is

known, the Wiener deconvolution filter can produce an equally good resolving kernel.

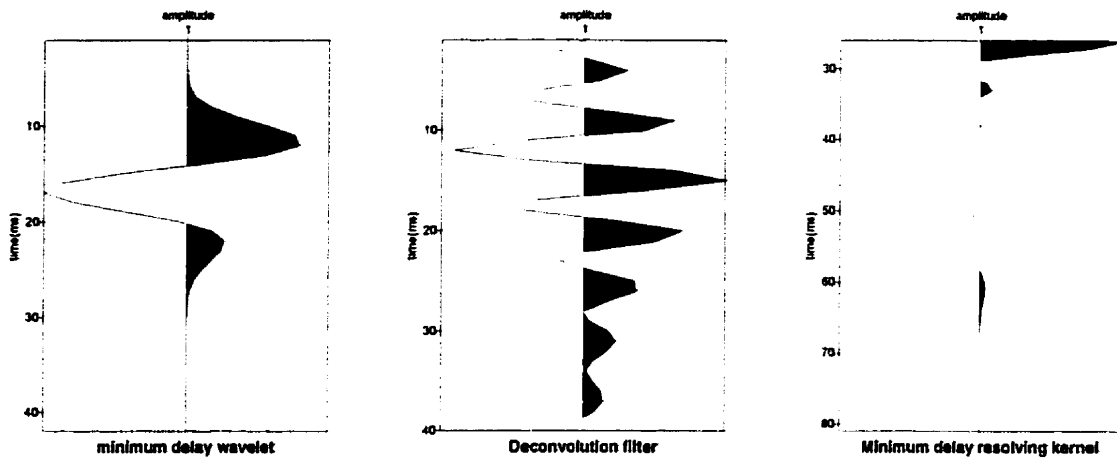


Figure 4.15: The model minimum delay wavelet,  $(-1.1 + z)^2(1.75 + z)^{38}$ , its deconvolution filter, and its resolving kernel. The optimal spiking position is at  $25ms$ .

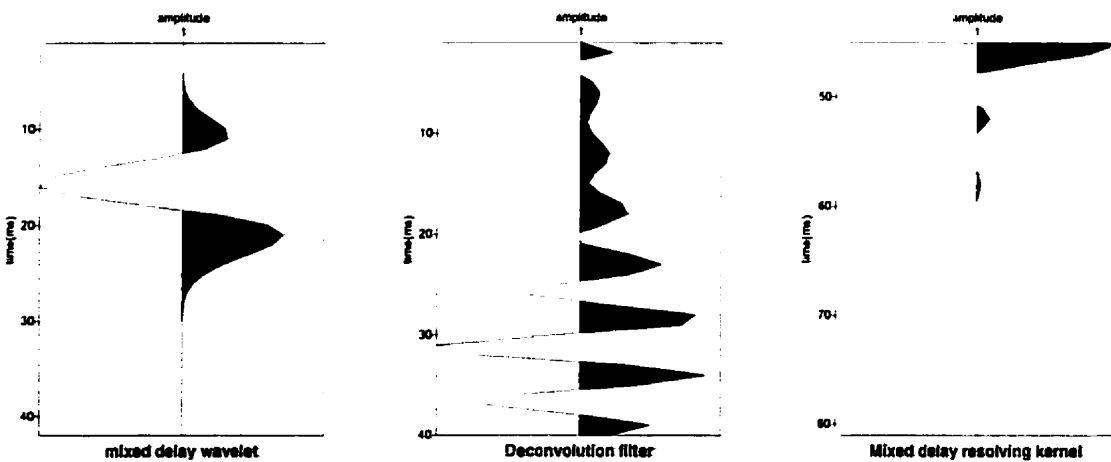


Figure 4.16: A mixed delay version of the model wavelet,  $(1 - 1.1z)^2(1.75 + z)^{38}$ , its deconvolution filter, and its resolving kernel. The optimal spiking position is at  $44ms$ .

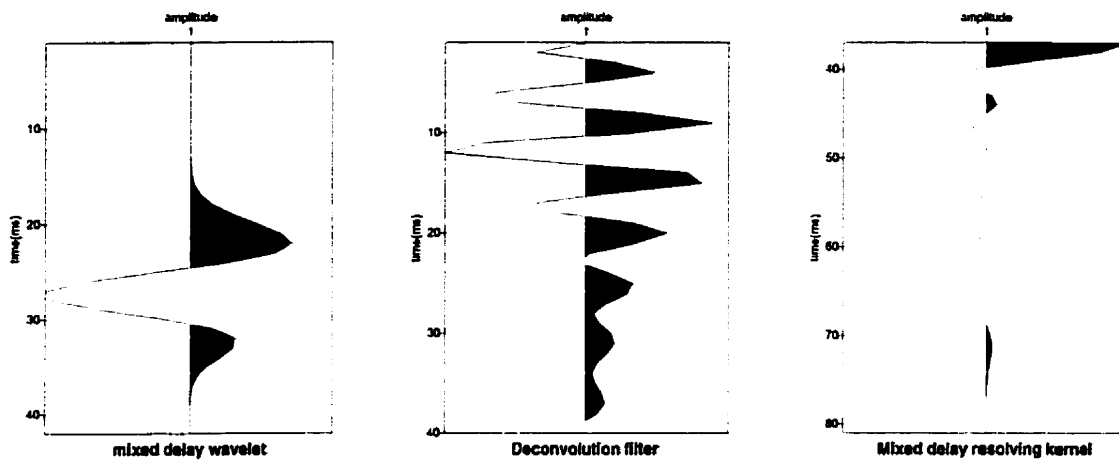


Figure 4.17: Another mixed delay version of the model wavelet,  $(-1.1 + z)^2(1 + 1.75z)^{38}$ , its deconvolution filter, and its resolving kernel. The optimal spiking position is at  $36ms$ .

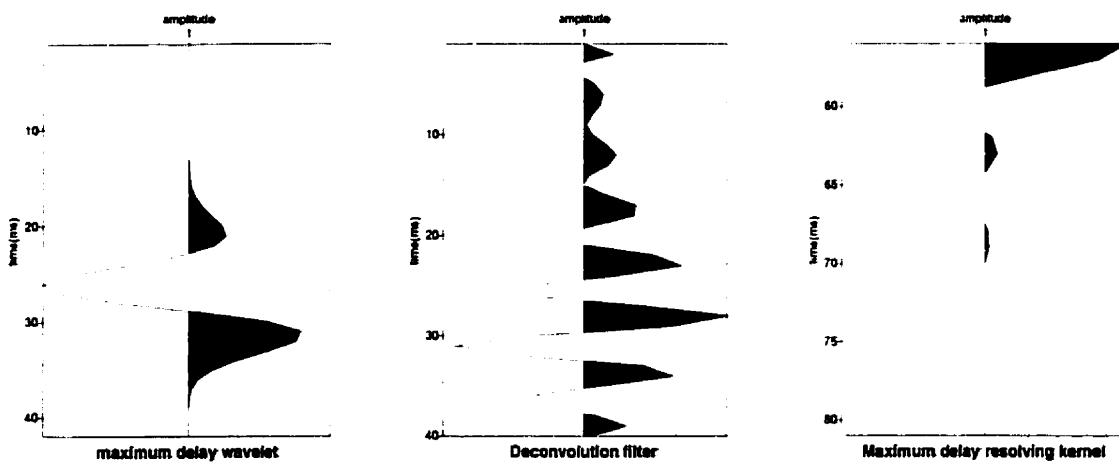


Figure 4.18: The maximum delay version of the model wavelet,  $(1 - 1.1z)^2(1 + 1.75z)^{38}$ , its deconvolution filter and its resolving kernel. The optimal spiking position is at  $55ms$ .

## 4.2.2 results: model 2

Figures 4.19 through 4.22 show the resolving kernel tests for the second model minimum phase wavelet and its selected permutations. The minimum phase wavelet has the *z-dipole* form  $(-1.35 + z)^2(1.5 + z)^{38}$  and the permutations considered are:  $(1 - 1.35z)^2(1.5 + z)^{38}$  (mixed delay),  $(-1.35 + z)^2(1 + 1.5z)^{38}$  (mixed delay), and  $(1 - 1.35z)^2(1 + 1.5z)^{38}$  (maximum delay).

In Figure 4.19, a spiking deconvolution filter for the minimum delay wavelet is shown along with the wavelet itself and the resulting resolving kernel. The convolution of the Wiener deconvolution filter with the wavelet produces the resolving kernel shown in this figure. This is a sharp resolving kernel with a narrow band-width. The optimal spiking position is at  $36ms$  and there is insignificant energy in the tail of the kernel. The front-loaded mixed delay wavelet is shown in Figure 4.20 and the deconvolution, in this case, produces a resolving kernel which is almost identical to the minimum phase situation with the exception being that now the optimal spiking position is at  $44ms$ . Notice that both of the resolving kernels shown thus far have a broad band-width. In Figure 4.21, the second mixed delay wavelet (end-loaded) has a sharp resolving kernel with slightly narrower band-width and an optimum spiking position at  $36ms$ . Figure 4.22 shows the resolving kernel result for the maximum delay wavelet. In this case, the kernel is sharp with a spiking position at  $44ms$  and the kernel has a narrow band-width.

With the wavelets used in this section, the trend hinted at earlier is again visible. As the delay in the wavelet is changed from minimum, through mixed, to maximum, it is seen that the optimum spiking position deviates to time positions equal to or later than the optimum

position seen for the minimum delay case. In addition, as before, these results show that if the wavelet is known, then the optimum Wiener–Levinson deconvolution filter will convolve with the wavelet in question to create a sharp resolving kernel. The key question now becomes the following: *if the wavelet is not known and certain wavelet phase assumptions must be made in order to perform seismic deconvolution, how well will the deconvolved traces estimate the earth's reflectivity?*

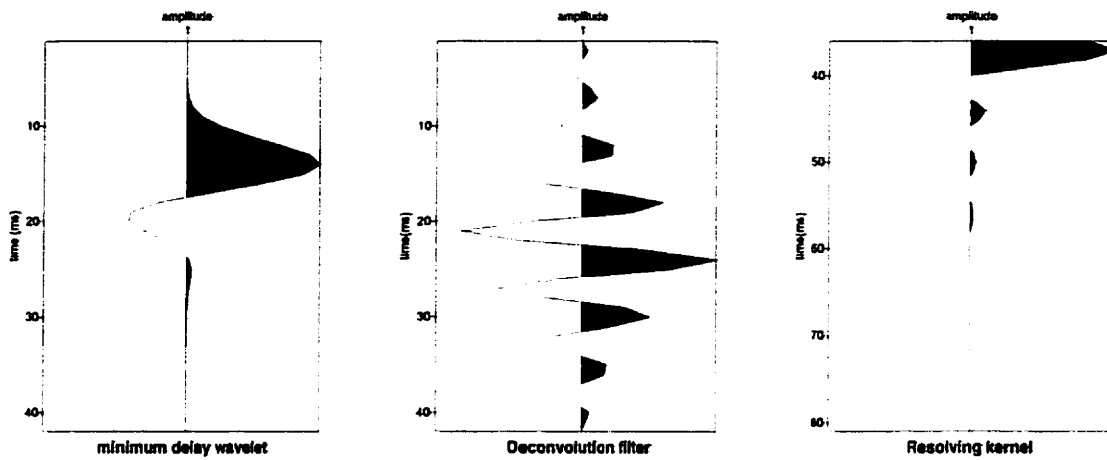


Figure 4.19: The model minimum delay wavelet,  $(-1.35 + z)^2(1.5 + z)^{38}$ , its deconvolution filter, and its resolving kernel. The optimal spiking position is at  $36ms$ .

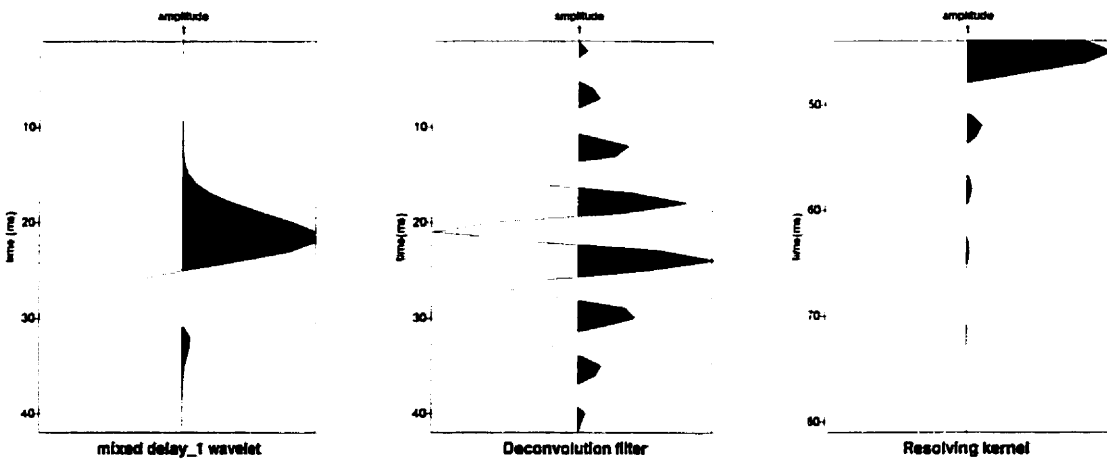


Figure 4.20: A mixed delay version of the model wavelet,  $(1 - 1.35z)^2(1.5 + z)^{38}$ , its deconvolution filter and its resolving kernel. The optimal spiking position is at  $44ms$ .

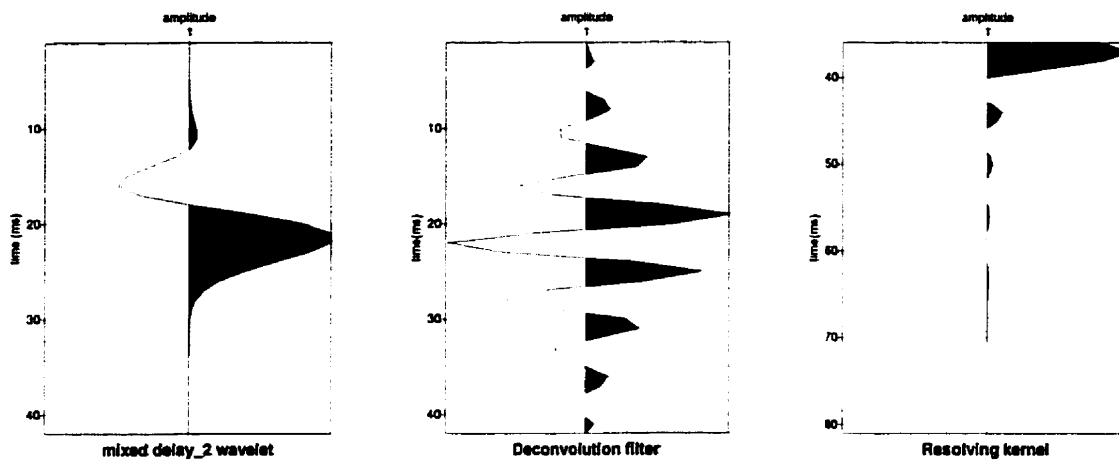


Figure 4.21: Another mixed delay version of the model wavelet,  $(-1.35 + z)^2(1 + 1.5z)^{38}$ , its deconvolution filter, and its resolving kernel. The optimal spiking position is at  $36ms$ .

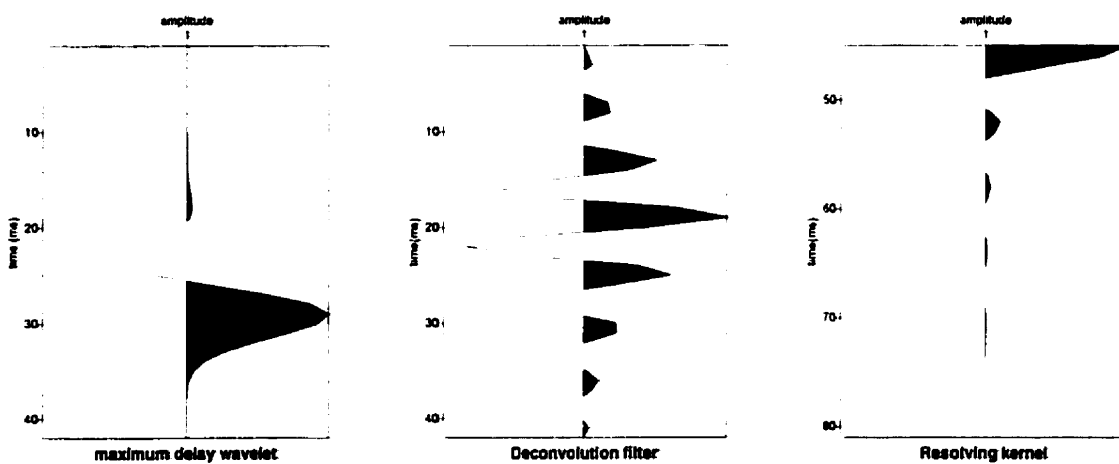


Figure 4.22: The maximum delay version of the model wavelet,  $(1 - 1.35z)^2(1 + 1.5z)^{38}$ , its deconvolution filter and its resolving kernel. The optimal spiking position is at  $44ms$ .

## 4.3 The well–log phase assumption test

The next 8 images display the effect of the minimum phase assumption on the deconvolution of the entire trace. For both models, each synthetic is created by the convolution of a wavelet (minimum, mixed, or maximum delay) with the model reflectivity sequence. In each of these models, the minimum delay trace is used to estimate minimum delay wavelets by the Hilbert transform and Wiener–Levinson double inverse methods.

### 4.3.1 results: model 1

This section introduces the problems that often arise when using the minimum phase assumption. Figures 4.23 through 4.26 illustrate just how problematic and damaging the minimum phase assumption can be. Shown in Figure 4.23 is the actual reflectivity sequence used in this analysis, the Hilbert transform deconvolution of the minimum delay trace, and the Wiener–Levinson deconvolution of the minimum delay trace. Both of these reflectivity estimates have a band–passed nature to them and suffer from significant amplitude attenuation. Both also seem to have strong impulses for minor reflections but the major reflectivities are absent. It also appears as if the Wiener–Levinson estimate suffers more from these shortcomings than the Hilbert transform estimate. Similar results are seen in Figure 4.24 where the results of a mixed delay trace deconvolution are presented. Present here are the same shortcomings listed previous except that there seems to be significant phase mismatch. Next (Figure 4.25) are the deconvolution results for the second mixed delay trace. These reflectivity estimates cannot, not even in the broadest sense, be considered representative of the model reflectivity. This may be due to the fact that both assumptions (phase and

randomness) about the wavelet are now being used in the deconvolution. The time delay is particularly noticeable. Finally, in Figure 4.26, there are the results of the deconvolutions for the maximum delay trace. Here, the statistical reflectivity estimates are very time delayed, have a significant band-passed nature, suffer from severe phase mismatches, and there is major amplitude attenuation.

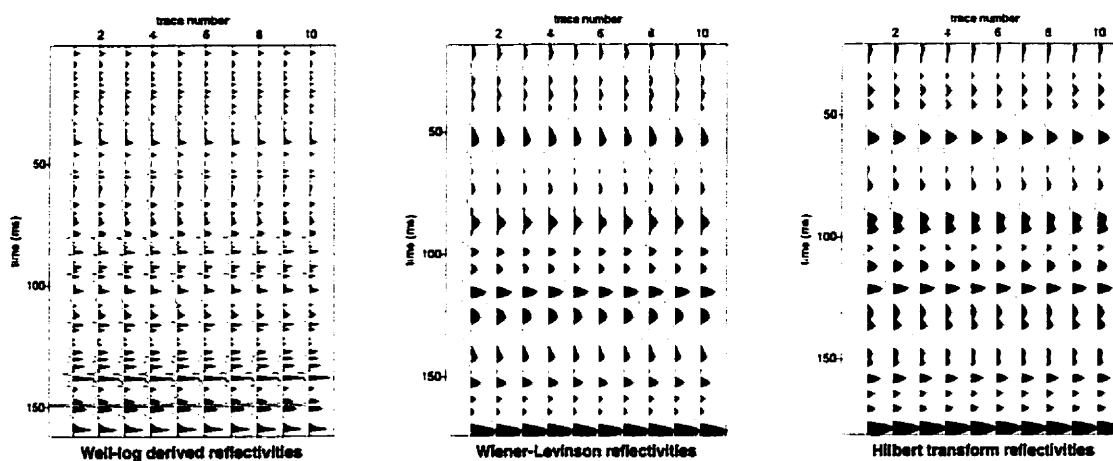


Figure 4.23: The actual reflectivity sequence (left), spiking deconvolution of the minimum delay synthetic trace based on the Wiener–Levinson wavelet (center), and spiking deconvolution of the minimum delay synthetic trace based on the Hilbert wavelet (right).

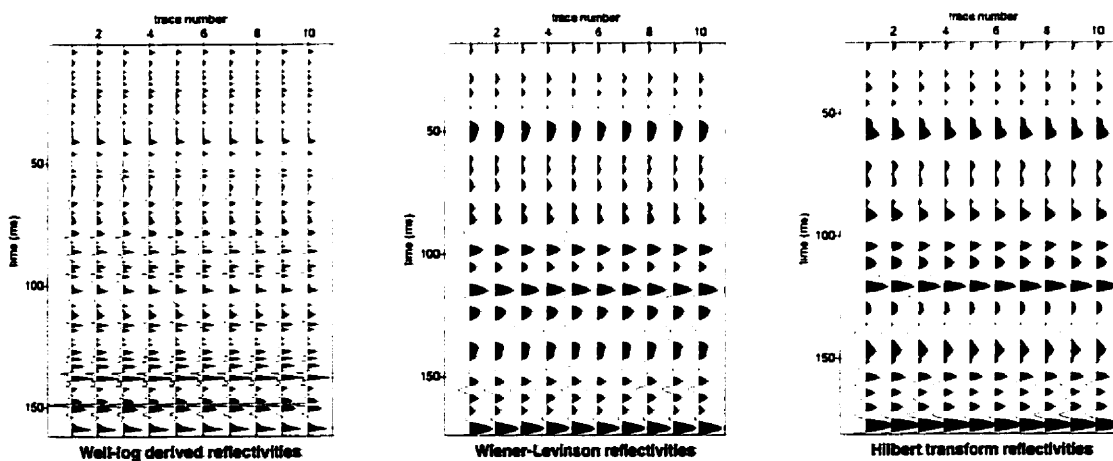


Figure 4.24: The actual reflectivity sequence (left), spiking deconvolution of the mixed delay synthetic trace based on the Wiener–Levinson wavelet (center), and spiking deconvolution of the mixed delay synthetic trace based on the Hilbert wavelet (right).

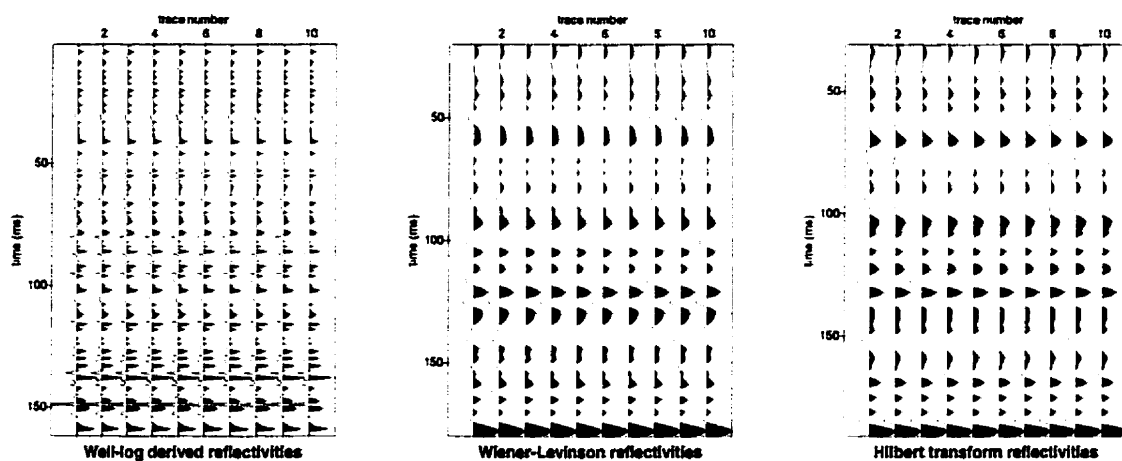


Figure 4.25: The actual reflectivity sequence (left), spiking deconvolution of the second mixed delay synthetic trace based on the Wiener-Levinson wavelet (center), and spiking deconvolution of the second mixed delay synthetic trace based on the Hilbert wavelet (right).

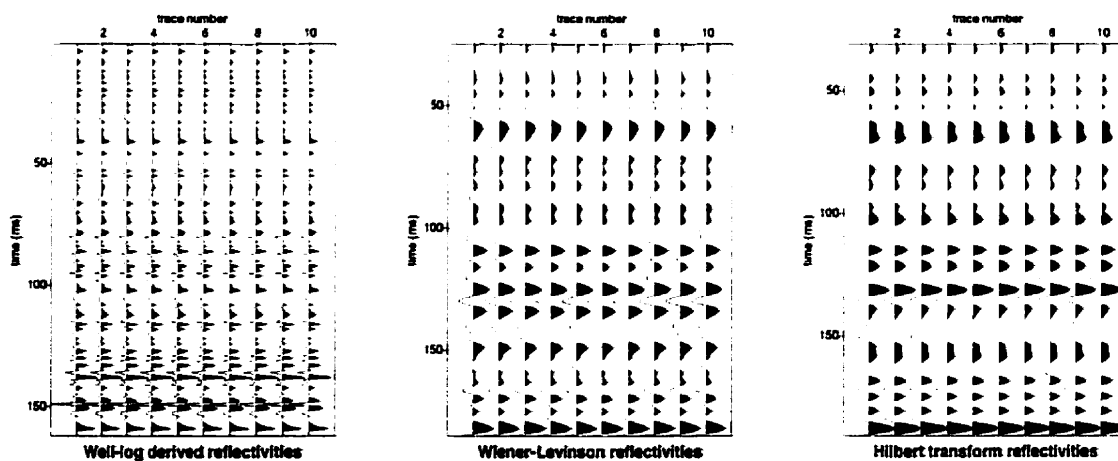


Figure 4.26: The actual reflectivity sequence (left), spiking deconvolution of the maximum delay synthetic trace based on the Wiener-Levinson wavelet (center), and spiking deconvolution of the maximum delay synthetic trace based on the Hilbert wavelet (right).

### 4.3.2 results: model 2

Figures 4.27 through 4.30 tell the same story seen in model 1. Shown in Figure 4.27 is the actual reflectivity sequence used in this analysis, the Hilbert transform deconvolution of the minimum delay trace, and the Wiener-Levinson deconvolution of the minimum delay trace. Both of these reflectivity estimates have a prominent band-passed nature to them, suffer from significant amplitude attenuation, and are time delayed. Both also seem to have strong impulses for minor reflections but the major reflectivities are absent. It also appears as if the Wiener-Levinson estimate suffers more from these short comings than the Hilbert transform estimate. Similar results are seen in Figure 4.28 where the results of a mixed delay trace deconvolution are presented. Present here are the same short comings listed previous except that there seems to be phase mismatch. Next (Figure 4.29) are the deconvolution results for the second mixed delay trace. These reflectivity estimates are not representative of the model reflectivity. The time delay is particularly noticeable but these estimates do not suffer from as much band-passing or amplitude attenuation. Finally, in Figure 4.30, there are the results of the deconvolutions for the maximum delay trace. Here, the statistical reflectivity estimates are very time delayed. However, the trace deconvolutions have better amplitude content than the first two of this subsection.

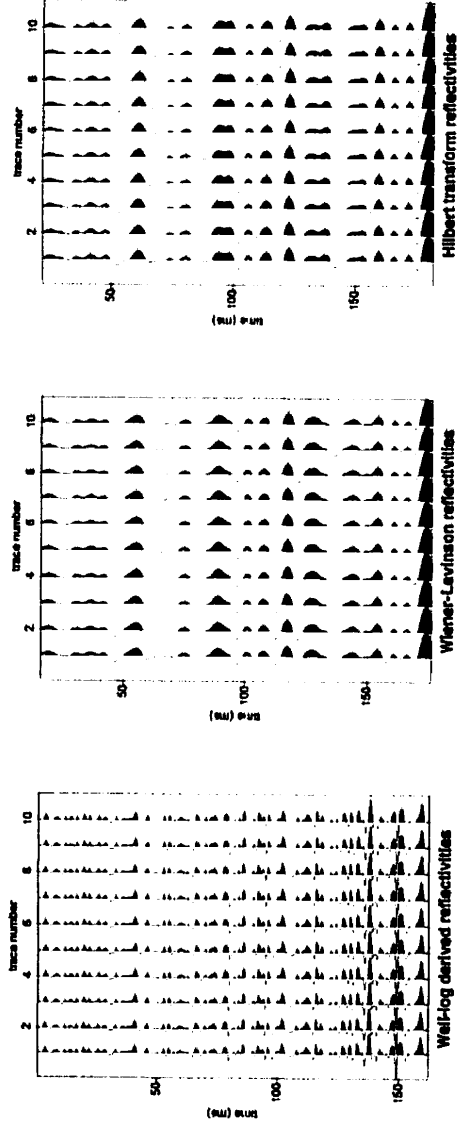


Figure 4.27: The actual reflectivity sequence (left), spiking deconvolution of the minimum delay synthetic trace based on the Wiener-Levinson wavelet (center), and spiking deconvolution of the minimum delay synthetic trace based on the Hilbert wavelet (right).

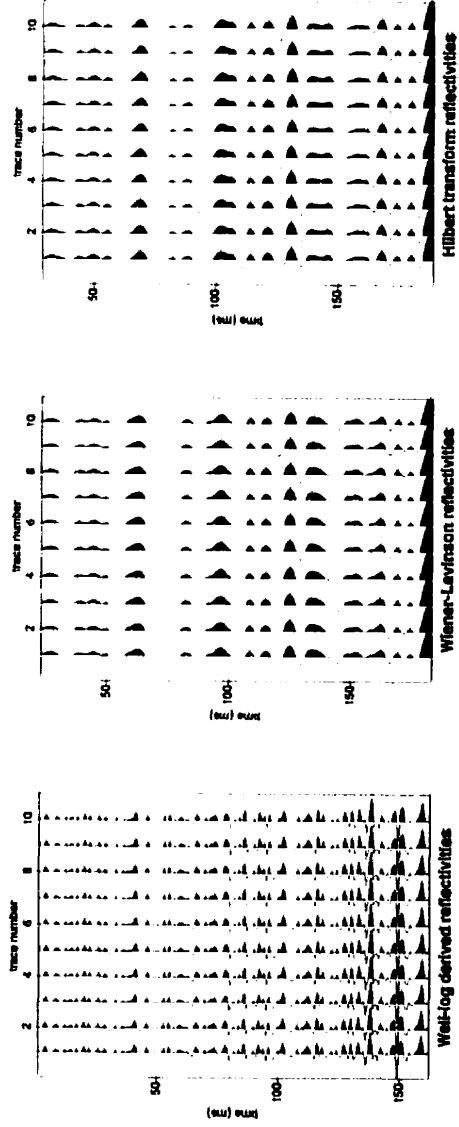


Figure 4.28: The actual reflectivity sequence (left), spiking deconvolution of the mixed delay synthetic trace based on the Wiener-Levinson wavelet (center), and spiking deconvolution of the mixed delay synthetic trace based on the Hilbert wavelet (right).

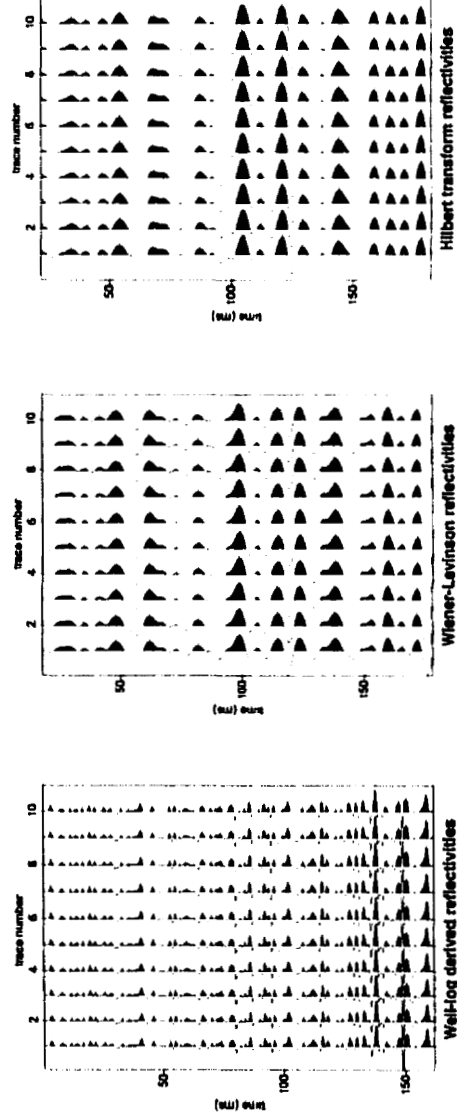


Figure 4.29: The actual reflectivity sequence (left), spiking deconvolution of the second mixed delay synthetic trace based on the Wiener-Levinson wavelet (center), and spiking deconvolution of the second mixed delay synthetic trace based on the Hilbert wavelet (right).

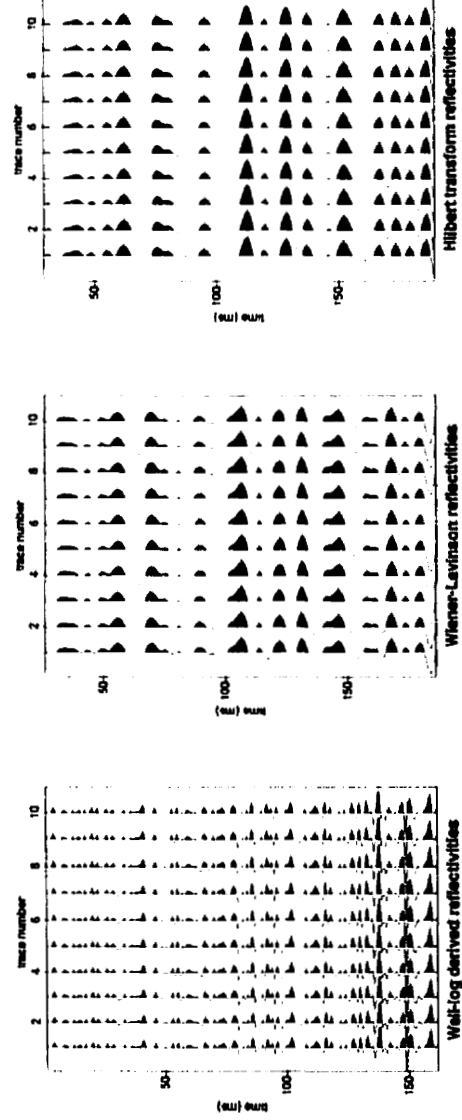


Figure 4.30: The actual reflectivity sequence (left), spiking deconvolution of the maximum delay synthetic trace based on the Wiener-Levinson wavelet (center), and spiking deconvolution of the maximum delay synthetic trace based on the Hilbert wavelet (right).

## 4.4 The phase assumption test

The final two subsections illustrate a set of results using the proposed test for phase discussed earlier. Both model 1 and model 2 use the synthetic traces to statistically estimate Wiener-Levinson deconvolution filters. These filters, computed using the minimum phase assumption, are then convolved with the actual wavelets to generate resolving kernels. The similarity to an ideal spike will give a measure of how well or how poor the minimum phase assumption is working.

### 4.4.1 results: model 1

Given the rather poor performance of the statistical methods in trace deconvolution section, another approach is taken. As described above, the model synthetic traces are used with the minimum phase assumption to spike the wavelets used in this model. That is, the synthetic traces generate the statistically estimated minimum phase filter that convolves with the actual wavelets to give a good resolving kernel where the major peak greatly dwarfs the residual peaks in the kernel. The intrigue in Figure 4.32 and Figure 4.33 comes from the mixed phase nature of the actual wavelets. Figure 4.32 shows a model mixed phase wavelet that is similar to the maximum delay wavelet (see Figure 4.34), except that the mixed delay wavelet is not as time delayed as the maximum delay wavelet. The mixed delay wavelet spikes at  $39ms$ , while the maximum delay wavelet spikes at  $49ms$ . Its resolving kernel is a version of the kernel for the maximum delay wavelet except at an earlier time. The same holds when considering the mixed delay wavelet in Figure 4.33 and the minimum delay wavelet (see Figure 4.31). This mixed delay wavelet has a close resemblance to the

minimum delay wavelet and its resolving kernel is that of the minimum delay wavelet but it spikes at  $22ms$  instead of  $11ms$ .

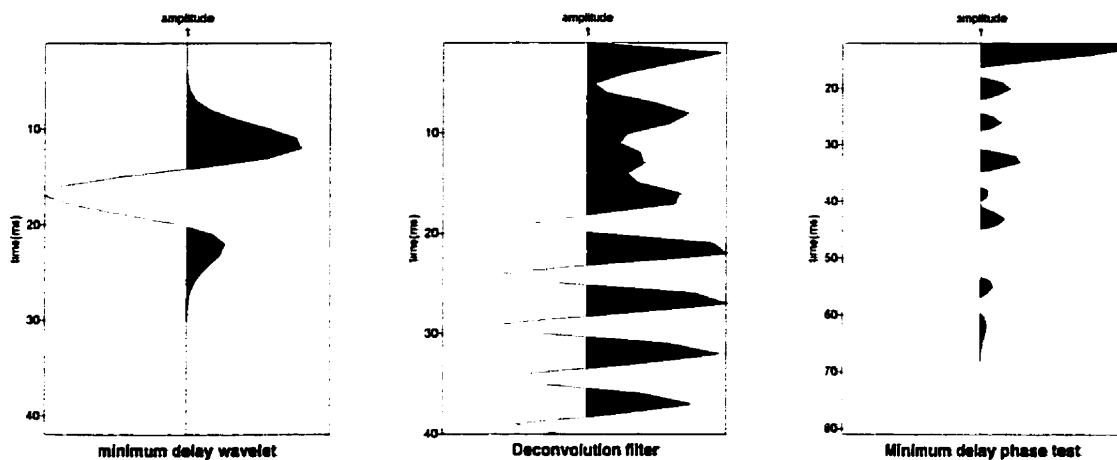


Figure 4.31: The actual minimum phase wavelet used to create the previously shown synthetic is convolved with the deconvolution filter, estimated from the synthetic trace, to give the resolving kernel to the right.

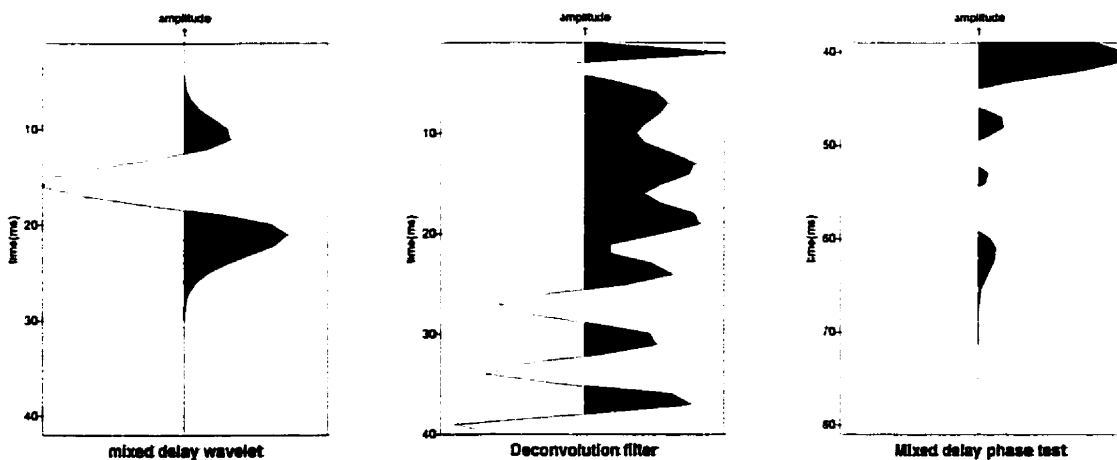


Figure 4.32: The actual mixed phase wavelet used to create the previously shown synthetic is convolved with the deconvolution filter, estimated from the synthetic trace, to give the resolving kernel to the right.

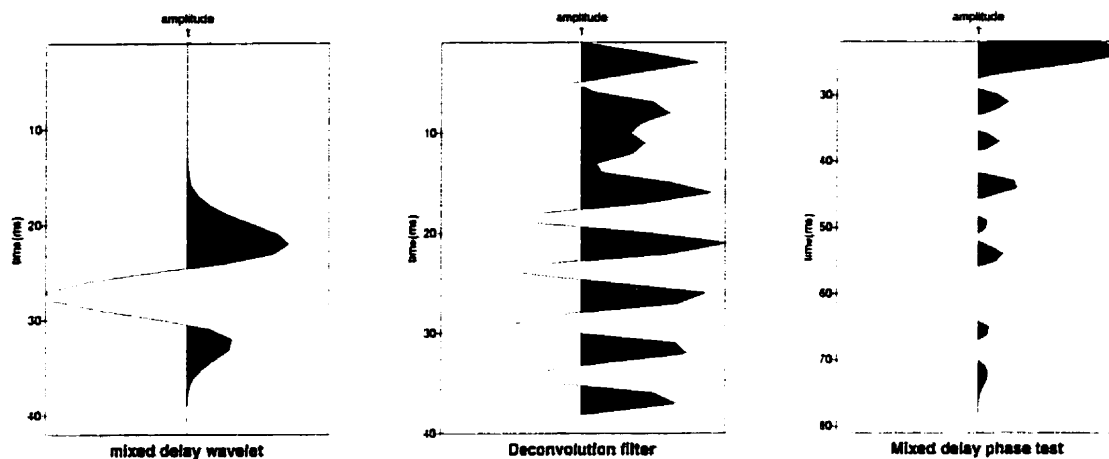


Figure 4.33: The actual mixed phase wavelet used to create the previously shown synthetic is convolved with the deconvolution filter, estimated from the synthetic trace, to give the resolving kernel to the right.

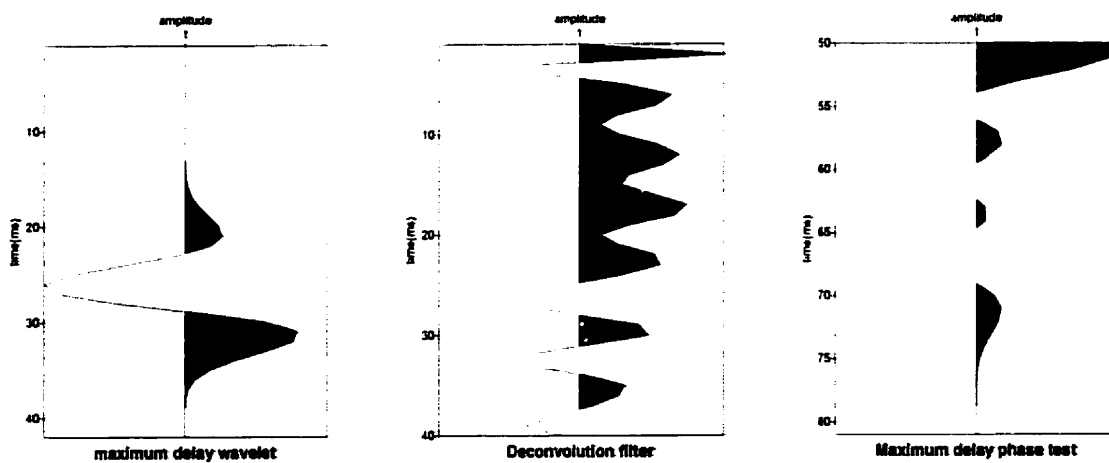


Figure 4.34: The actual maximum phase wavelet used to create the previously shown synthetic is convolved with the deconvolution filter to give the resolving kernel to the right.

#### 4.4.2 results: model 2

The pattern identified with the previous model also reappears in these result. Again it is seen that one mixed delay wavelet follows the patterns of the minimum delay wavelet while the other mimics the maximum delay wavelet's behavior. The general trend being seen with these two simple models is that even if the wavelet is not minimum phase the deconvolution filter based on the minimum phase assumption will effectively convert the mixed delay wavelet to a spike.

The intrigue seen in the previous subsection is seen again here. Figure 4.36 shows a model mixed phase wavelet that is similar to the minimum delay wavelet (see Figure 4.35), except that it is more time delayed. The mixed delay wavelet spikes at  $23ms$ , while the minimum delay wavelet spikes at  $14ms$ . Its resolving kernel is a version of the kernel for the minimum delay wavelet except at a later time. The same holds when considering the mixed delay wavelet in Figure 4.37 and the maximum delay wavelet (see Figure 4.38). This mixed delay wavelet has a close resemblance to the maximum delay wavelet and its resolving kernel is that of the maximum delay wavelet but it spikes at  $35ms$  instead of  $36ms$ .

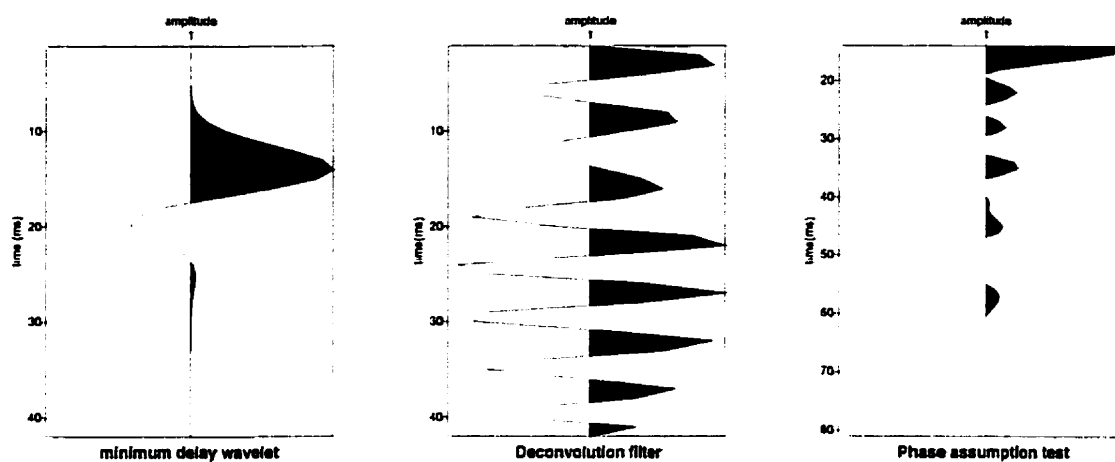


Figure 4.35: The actual minimum phase wavelet used to create the previously shown synthetic is convolved with the deconvolution filter, estimated from the synthetic trace, to give the resolving kernel to the right.

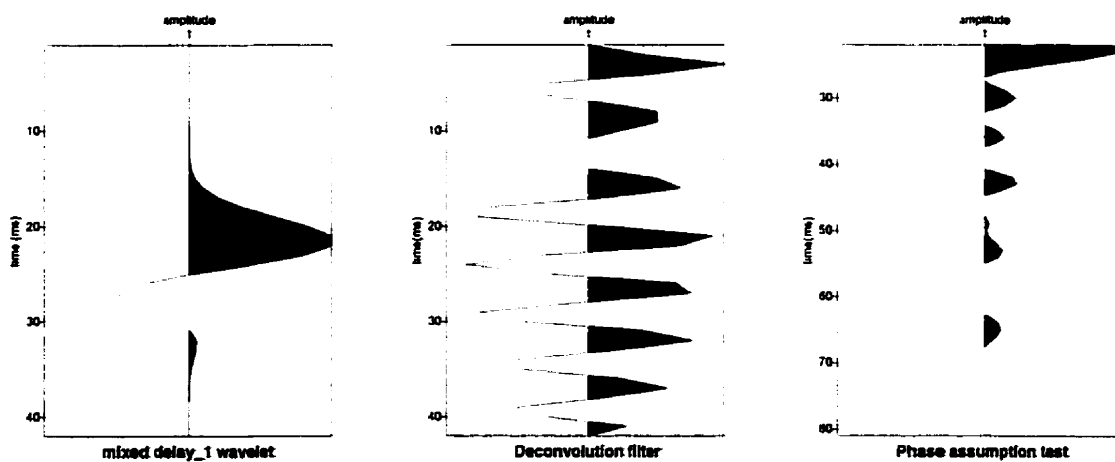


Figure 4.36: The actual mixed phase wavelet used to create the previously shown synthetic is convolved with the deconvolution filter, estimated from the synthetic trace, to give the resolving kernel to the right.

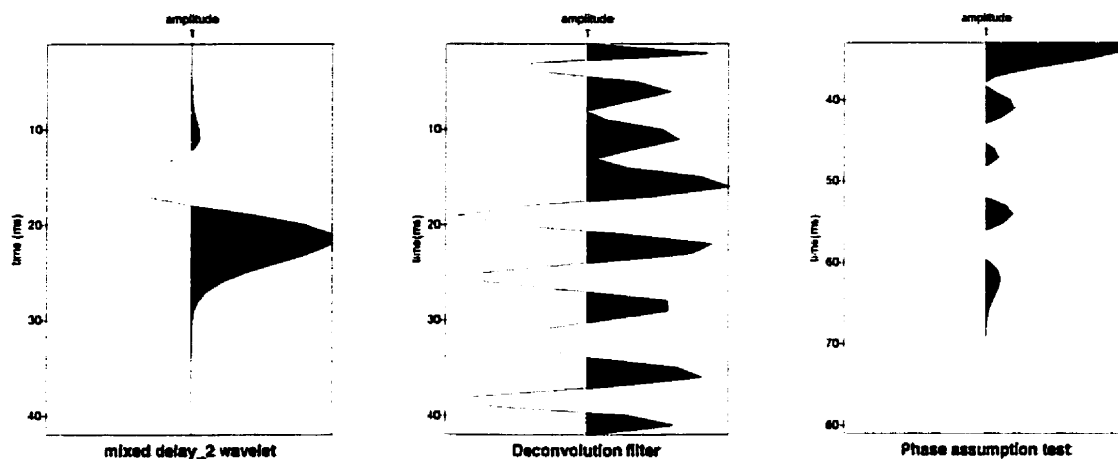


Figure 4.37: The actual mixed phase wavelet used to create the previously shown synthetic is convolved with the deconvolution filter, estimated from the synthetic trace, to give the resolving kernel to the right.

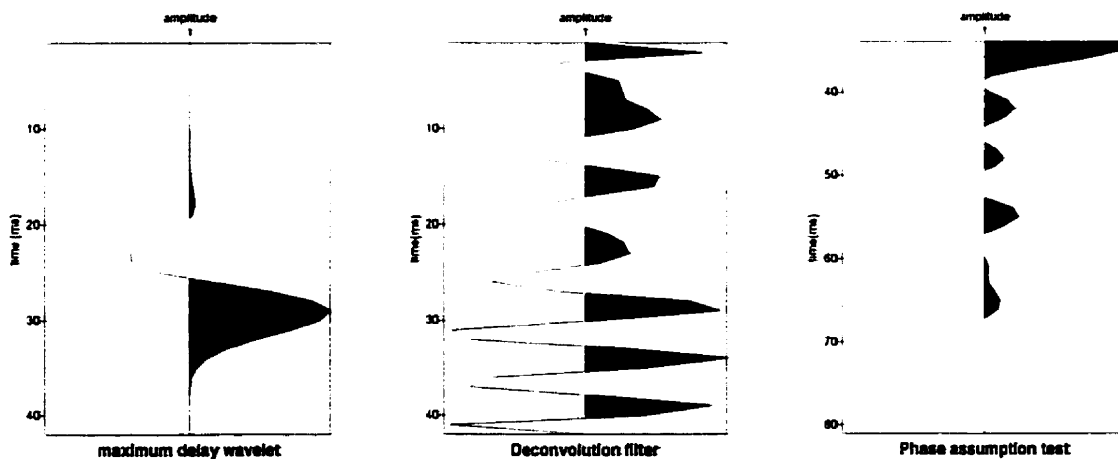


Figure 4.38: The actual maximum phase wavelet used to create the previously shown synthetic is convolved with the deconvolution filter, estimated from the synthetic trace, to give the resolving kernel to the right.

# Chapter 5

## Conclusions

The preceding results of Chapter 3 shed some light on the issue of the randomness of the reflectivity sequence. Use of sonic and density logs to compute a reflectivity sequence serves to locally measure the goodness of the statistical estimates and helps to test the validity of the assumption. In order to evaluate the effectiveness of the random reflectivity assumption on deconvolution, a simple test is proposed based on the use of a sonic log. Also investigated are the various resolving kernels. The closeness of the resolving kernel to a spike is a measure of the deconvolution filter's effectiveness. A further test is to apply the estimated deconvolution filter to the trace and compare the deconvolved output to the reflectivity sequence. With real data, we can compare the wavelet estimate obtained from surface recorded data with waveforms obtained from in-situ VSP recordings. Through all of the randomness investigations, it has become clear that the justification of the randomness assumption is closely tied to the lithology of an area. That is to say, if the rock layering has periodic properties, then its reflectivity sequence will not exhibit the required randomness property. Should reflectivity randomness be an inadequate assumption, then the processing

flow will need to resort to alternate methods or, in fact, to physical measurements of the source signature.

From the investigations of Chapter 4, it is clear the minimum phase assumption is far more critical in determining the success or failure of statistical deconvolution methods. Proper investigation of the minimum phase assumption must be done in a synthetic framework because a knowledge of how the wavelet phase differs from minimum phase is required to know how these phase differences affect statistical deconvolution. The complete picture involves investigating resolving kernels and trace deconvolutions. It is evident that if there is *a priori* knowledge of the wavelet, then the statistical methods used in this thesis will consistently produce a well-defined, sharp, resolving kernel. Also seen from the study is that statistically estimating minimum phase wavelets from input traces and then using these wavelets to deconvolve the trace is a disastrous path to follow. Far better results are seen when the statistical deconvolution filters are estimated from the trace themselves. This is seen by convolving the filter estimated from the trace with the actual wavelet used to create the trace. For the situations considered in this thesis, the previous process creates good resolving kernels and, therefore, it can be concluded that the filters will effectively spike the embedded wavelet.

As a whole, for the Alberta data examined in this thesis, it is seen that the problems of wavelet phase and wavelet non-stationarity beset the statistical deconvolution problem far more than the random reflectivity assumption. To assess the usefulness of statistical deconvolution as a processing tool, use the proposed tests along with the best interpretive judgment available.

## REFERENCES

- [1] Bednar, J. B., 1983, Applications of median filtering to deconvolution, pulse estimation, and statistical editing of seismic data: *Geophysics*, 48, 1598 – 1610.
- [2] Claerbout, J., 1976, *Fundamentals of seismic data processing*: McGraw-Hill, New York, New York.
- [3] Danielsen, V., and T. V. Karlsson, 1984, Extraction of signatures from seismic and well data: *First Break*, 2, 15 – 22.
- [4] Futterman, W. I., 1962, Dispersive body waves: *Journal of Geophysical Research*, 67, 5279 – 5291.
- [5] Gal'perin, E. I., 1985, *Vertical seismic profiling*: SEG, Tulsa, Oklahoma.
- [6] Klauder, J. R., A. C. Price, S. Darlington, and W. J. Albersheim, 1960. The theory and design of chirp radars: *Bell System Technical Journal*, 39, 745 – 807.
- [7] Lindsey, J. P., 1987, Measuring wavelet phase from seismic data: SEG 1987 fall distinguished lecture.
- [8] Lindsey, J. P., 1996, A note on phase unwrapping: *Geophysics reprint series*, # 18, 301 – 307.
- [9] Lines, L. R., and S. Treitel, 1991, Wavelets, well-logs, and Wiener filters: *First Break*, 3, 9 – 14.
- [10] Lines, L. R., and T. J. Ulrych, 1977, The old and the new in seismic deconvolution and wavelet estimation: *Geophysical Prospecting*, 25, 512–540.
- [11] Ristow, D., and D. Jurczyk, 1974, Vibroseis deconvolution: *Geophysical Prospecting*, 23, 363 – 379.

- [12] Robinson, E. A., 1967a, *Multichannel time series analysis*: Holden Day, San Francisco, California.
- [13] Robinson, E. A., 1967b, Predictive decomposition of time series with application to seismic exploration: *Geophysics*, 32, 418–484.
- [14] Robinson, E. A., and S. Treitel, 1980, *Geophysical signal analysis*: Prentice–Hall, Englewood Cliffs, New Jersey.
- [15] Russell, B., 1994, *Seismic inversion*: SEG course notes.
- [16] Schoepp, A., 1998, *Improving seismic resolution with nonstationary deconvolution*: Master's Thesis, Department of Geology and Geophysics, University of Calgary, Calgary, Alberta.
- [17] Sheriff, R. E., 1974, *Encyclopedic dictionary of exploration geophysics*: SEG, Tulsa, Oklahoma.
- [18] Sheriff, R. E. and L. P. Geldart, 1995, *Exploration seismology*: 2<sup>nd</sup> edition, Cambridge University Press, New York, New York.
- [19] Telford, W. M., L. P. Geldart, and R. E. Sheriff, 1990, *Applied geophysics*: 2<sup>nd</sup> edition, Cambridge University Press, New York, New York.
- [20] Treitel, S., and L. R. Lines, 1982, Linear inverse theory and deconvolution: *Geophysics*, 47, 1153 – 1159.
- [21] White, R. E., and P. N. S. O'Brien, 1974, Estimation of the primary seismic pulse: *Geophysical Prospecting*, 22, 627 – 651.
- [22] Yilmaz, O., 1987, *Seismic data processing*: SEG, Tulsa, Oklahoma.
- [23] Ziolkowski, A., 1991, Why don't we measure seismic signatures?: *Geophysics*, 56, 190 – 201.